Ground state of a two-dimensional electron liquid in a weak magnetic field

M. M. Fogler, A. A. Koulakov, and B. I. Shklovskii
Theoretical Physics Institute, University of Minnesota, 116 Church Street Southeast, Minneapolis, Minnesota 55455
(Received 23 January 1996; revised manuscript received 26 March 1996)

We consider a clean two-dimensional electron liquid in a weak magnetic field where $N \gg 1$ lower Landau levels are completely filled, while the upper level is only partially filled. Due to a screening by the lower Landau levels, the repulsive interaction between any two electrons at the upper level as a function of the separation between the guiding centers of their cyclotron orbits abruptly drops at the distance of two cyclotron radii. Such a ''box-like'' component in the interaction potential makes the uniform distribution of the electron density at the upper Landau level unstable, and domains with filling factor equal to one and zero are formed. The shape of domains is studied both analytically and numerically. We show that when the filling factor of the upper Landau level is close to one-half, the domains have the form of parallel stripes alternating with a spatial period close to three cyclotron radii. Away from a small interval around half-filling, a ''bubble'' phase is more favorable. We investigate the implications of the proposed ground state for the one-particle density of states, which can be probed by tunneling experiments. For the stripe phase, the density of states is shown to have a pseudogap linearly dependent on the magnetic field in the limit of large N. [S0163-1829(96)00227-5]

I. INTRODUCTION

Since the discovery of the integer and fractional quantum Hall effects,[1] the description of the ground state of an interacting two-dimensional (2D) electron gas in a magnetic field became one of the central problems of condensed matter physics. The main difficulty of this problem is related to the fact that the electron gas in the magnetic field is highly degenerate and, therefore, the Coulomb interaction cannot be considered as a small perturbation.

In a pioneering work made even before the discovery of the quantum Hall effect, Fukuyama, Platzman, and Anderson[2] found that in a quantum limit where only one Landau level (LL) is partially occupied, a uniform uncorrelated spin-polarized electron liquid is unstable against the formation of a charge density wave (CDW). Later, Yoshioka and Fukuyama and also Yoshioka and Lee[3] claimed that the optimal period of the CDW coincides with that of the classical Wigner crystal (WC). In both works, the Hartree-Fock (HF) approximation has been used. The difference of the proposed HF WC state from a classical WC of pointlike particles is that the electrons are smeared over a distance of the order of the magnetic length $l=\hbar/\sqrt{m\omega_c}$ around the sites of the WC lattice. The WC ground state, however, failed to explain the fractional quantum Hall effect occurring when the filling factor $\nu=k_F^2 l^2$ is a simple rational fraction (here k_F is the Fermi wave vector of the 2D gas in zero magnetic field).

The explanation was made possible when Laughlin[4] suggested a non-HF trial state of uniform density for $\nu=\frac{1}{3},\frac{1}{5}$, which turned out to be a few percent lower in energy. Thus, although the HF approximation gives a rather accurate estimate of the energy, it fails to describe important electron-electron correlations at a partially filled lowest LL.

In the works discussed above, the ground state has been always assumed to be spin polarized. Recently, this requirement also has been reconsidered. It was found that a partially filled lowest LL may contain skyrmions.[5]

In this paper we consider the case of weak magnetic fields or high LL numbers N. A short version of this work[6] was published before.

There is growing evidence from analytical and numerical calculations that both the fractional states and skyrmions are restricted to the two lowest LL's ($N=0,1$) only (see Refs. 7–9). This point of view is also consistent with experiment because none of those structures has yet been observed at $N>1$ to our knowledge. Denote by $\overline{\nu_N}$ the filling of the upper LL, $\overline{\nu_N}=\nu-2N$. We will assume that (i) at $\overline{\nu_N}\leqslant 1$ the upper LL is completely spin polarized and (ii) the HF approximation gives an adequate description of the system.

Our theory strongly relies on the existence of Landau levels. In other words, we assume that even in weak magnetic fields, where the cyclotron gap $\hbar\omega_c$ is small, the electron-electron interactions do not destroy the Landau quantization. Certainly, this is far from being evident. On the mean-field level, the following argument can be given. (For a discussion of quantum fluctuations, see the paper by Aleiner and Glazman.[9]) The LL's survive if the absolute value of the interaction energy per particle at the upper LL is much smaller than $\hbar\omega_c$. The largest value of the interaction energy is attained at $\overline{\nu_N}=1$ where the electron density at the upper LL is the largest. It is equal to $-\frac{1}{2}E_{\rm ex}$, where $E_{\rm ex}$ is the exchange-enhanced gap for the spin-flip excitations[10] at $\overline{\nu_N}=1$ (it determines, e.g., the activation energy at the minima between spin-resolved resistivity peaks). The magnitude of this gap is given by[9]

$$E_{\rm ex}=\frac{r_s\hbar\omega_c}{\sqrt{2\pi}}\ln\left(\frac{2\sqrt{2}}{r_s}\right)+E_h, \quad r_s\ll 1, \tag{1}$$

where E_h is the ''hydrodynamic'' term[11]

$$E_h=\hbar\omega_c\frac{\ln(Nr_s)}{2N+1}. \tag{2}$$

The parameter r_s entering these formulas is defined by $r_s=\sqrt{2}/k_F a_B$, $a_B=\hbar^2\kappa/me^2$ being the effective Bohr radius. Therefore, in the considered limit $r_s \ll 1$ the LL's are indeed preserved. In practice $r_s \sim 1$ but even at such r_s the ratio $\alpha=E_{\rm ex}/\hbar\omega_c$ is still rather small. Experimentally, this ratio can be estimated to be near 0.25 at $0 \leqslant N \leqslant 4$.[12]

Let us now turn to the main subject of the paper, a partially filled upper LL. Due to the electron-hole symmetry within one spin subband, it suffices to consider only $0<\overline{\nu_N} \leqslant \frac{1}{2}$.

We want to find the ground state of a partially filled LL. As we just saw, the cyclotron motion is quantized. Thus, the remaining degrees of freedom are associated with the guiding centers of the cyclotron orbits. In the ground state these centers must arrange themselves in such a way that the interaction energy is the lowest. This prompts a quasiclassical analogy between the partially filled LL and a gas of ''rings'' with repulsive interaction, the radius of each ring being equal to the cyclotron radius, $R_c=\sqrt{2N+1}\,l$. Strictly speaking, the guiding center cannot be localized a single point, and so our analogy is not precise. However, there exists a single-electron state[13] (so-called coherent state) in which the guiding center has a very small scatter (of order l) around a given point. (For a more detailed description of such a state, see Sec. IV.) At large N where $l \ll R_c$, the proposed analogy becomes rather accurate. Since the rings repel each other, it is natural to guess that they form the WC. A trial wave function for this state was written by Aleiner and Glazman[9] by generalizing the Maki-Zotos $N=0$ wave function[14] to arbitrary N:

$$|\Psi\rangle=\prod_i c^\dagger_{\boldsymbol{R}_i}|0_N\rangle, \tag{3}$$

where $|0_N\rangle$ stands for N completely filled LL's, $c^\dagger_{\boldsymbol{R}}$ is the creation operator for a coherent state,[13] and $\boldsymbol{R}_i$ are the lattice sites of the classical WC with density $\overline{\nu_N}/(2\pi l^2)$. When $\overline{\nu_N}$ is small, $\overline{\nu_N} \ll 1/N$, the rings centered at neighboring lattice sites do not overlap and the concept of the WC is perfectly justified. However, at larger $\overline{\nu_N}$ they overlap strongly. In this work we show that at $\overline{\nu_N} \gg 1/N$ the ground state is completely different. Generally speaking, the structure of the ground state depends on r_s. In this section we discuss the results only for the practically important case, $r_s>0.06$. We found that in the range $1/N \lesssim \overline{\nu_N}<\overline{\nu_N^*}$ where $\overline{\nu_N}$ is somewhat smaller than $\frac{1}{2}$, the electrons form a ''super'' WC [Fig. 1(a)] of large domains (''bubbles'') containing about three $\overline{\nu_N}N$ electrons each and separated by the distance that slowly changes from $2R_c$ near the lower end of this range of $\overline{\nu_N}$ to approximately $3.3R_c$ near the upper end. At larger $\overline{\nu_N}$, $\overline{\nu_N^*}<\overline{\nu_N} \leqslant \frac{1}{2}$, the ''bubbles'' merge into parallel stripes [Fig. 1(b)] with the spatial period of approximately $2.7R_c$. The transition point $\overline{\nu_N^*}$ depends on N. In the limit of large N, it approaches the value of 0.4.

Domain patterns shown in Fig. 1 are well known in many other physical and chemical systems,[15] examples of the former being type I superconducting films in their intermediate state and magnetic films. We will refer to the patterns in Figs. 1(a) and 1(b) as the ''bubble'' and ''stripe'' phases, respectively.

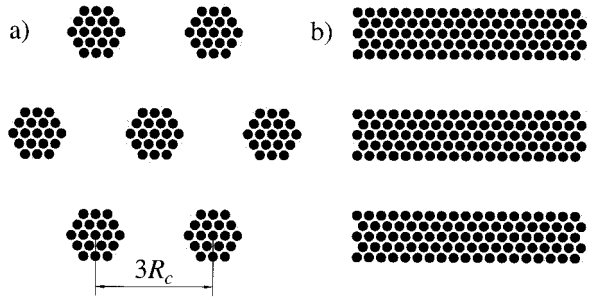

FIG. 1. (a) ''Bubbles.'' (b) ''Stripes.'' The black dots represent the guiding centers of cyclotron orbits.

It is, perhaps, surprising that the repulsive interaction leads to the formation of compacted clusters. In Sec. II we study this phenomenon in more detail and derive a general criterion for the interaction potential to have this property.

To understand why the clusterization occurs in the considered system, it is important to keep in mind the distinction between the local density of the guiding centers (i.e., the filling factor) and the local charge density. Despite the former being very inhomogeneous, the variations of the latter are rather small (of the order of 20%). In other words, our CDW state is not a conventional charge density but rather a guiding center density wave. This surprising property is a result of the ringlike shape of the electronic wave functions. Recall now that the energy of the system can be presented as the difference of the Hartree and the exchange terms. The inhomogeneity makes both of them increase relative to their uniform state values. However, the Hartree energy is sensitive only to the charge density variations and, therefore, it does not increase too much. On the other hand, for the exchange energy the variations in the filling factor are important, and it increases considerably, making the CDW state more favorable.

For not too small $\overline{\nu_N}$, the cohesive energy of our state is of the order of the exchange gap $E_{\rm ex}$. For example, the cohesive energy at $\overline{\nu_N} \sim \frac{1}{2}$ and $r_s \sim 1$ is given by

$$E_{\rm coh}^{\rm CDW} \approx -\frac{r_s}{8\sqrt{2}\pi}\hbar\omega_c \ln\left(1+\frac{0.3}{r_s}\right)-\frac{E_h}{4}$$

$$\approx -0.01\hbar\omega_c-\frac{E_h}{4}. \tag{4}$$

The last line in this equation corresponds to the case $r_s \sim 1$, where the logarithmic factor can be expanded.

By the term cohesive energy we mean the difference in the energies per particle at the upper LL in the given state and in the uniform uncorrelated electron liquid (appropriate at very high temperature).

One can argue also that our CDW state turns out to be the most energetically favorable because it possesses the optimal correlations on the largest length scale in the problem, R_c. The correlations on the length scale l, built into the structure of, say, the WC, are much less effective. We believe that for the same reason at large N the Laughlin liquids cannot compete with the CDW state either.

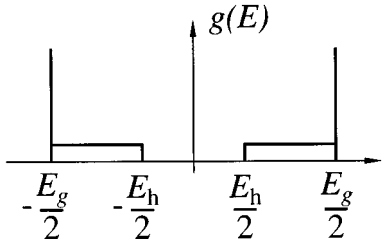

FIG. 2. The DOS for the stripe CDW in the limit of large N (schematically).

One of the important properties of the proposed ground state is a pseudogap in its one-particle density of states (DOS). We call it a pseudogap because although the DOS does not actually vanish, it appears small between two sharp peaks at the extremes of the spectrum (see Fig. 2). Such peaks are the particular form of the Van Hove singularities. The distance between the peaks (the width of the pseudogap) for $\overline{\nu_N}\sim\frac{1}{2}$ is equal to

$$E_g\approx\frac{r_s\hbar\omega_c}{\sqrt{2}\pi}\ln\left(1+\frac{0.3}{r_s}\right)+E_h\approx 0.07\hbar\omega_c+E_h, \qquad (5)$$

which is very close to $E_{\rm ex}$.

Besides the peaks, the DOS has an additional structure, such as a shallow gap of width E_h centered at the Fermi energy. The existence of such a gap was predicted in Refs. 9 and 19.

Figure 2 depicts the asymptotical form of the DOS at truly large N. At moderate N, the DOS appears merely as two distinct peaks. The reason for this is that the difference between E_g and E_h is not too large yet, while the Van Hove singularities are not extremely sharp. As a result, the intervals $\frac{1}{2}E_h<|E|<\frac{1}{2}E_g$ of constant $g(E)$ (see Fig. 2) are totally absorbed by the Van Hove peaks.

The proposed ground state enables us to explain two interesting experimental findings. One is a pseudogap in the tunneling DOS first observed in the experiments with single quantum well[16] systems and, recently, with double quantum well systems.[17,18] It was found that the differential conductivity as a function of the bias voltage exhibits two maxima. The distance $E_{\rm tun}$ between the maxima appears to be linear in magnetic field.[18] We show that the dependence of $E_{\rm tun}$ on the magnetic field is more complicated. However, in the experimental range $N\leqslant 4$, it can be satisfactorily fitted to the linear law $E_{\rm tun}\approx 0.4\hbar\omega_c$, which compares favorably with the experimental value of $0.45\hbar\omega_c$.[18]

Another important application of the proposed picture concerns the conductivity peak width of the integer quantum Hall effect in high-mobility structures. It is usually assumed that the disorder in such systems is long ranged. In this case the semiclassical electrostatic model of Efros[21] predicts that the electron liquid is compressible in a large fraction of the sample area. If compressible liquid is considered to be metallic, then the conductivity peaks are necessarily wide,[21] which is indeed the case at relatively high temperatures.[22] However, it is well known that at low temperatures the peaks are narrow, which may be interpreted as the pinning of the compressible liquid by the disorder.[23] The crystalline structure of the compressible liquid (Fig. 1) makes such a pinning possible even though the disorder is long ranged. When the compressible liquid is pinned, it cannot move as a whole. As a result, σ_{xx} vanishes at all $\overline{\nu_N}\neq\frac{1}{2}$. Precisely at $\overline{\nu_N}=\frac{1}{2}$, however, another mechanism of the transport becomes operational.[24] It is related to the propagation of quasiparticles along the boundaries of the domains with $\nu_N=1$ and 0, sometimes referred to as ''bulk edge states.'' The dc transport is possible only when the bulk edge states percolate through the sample. This is realized only at $\overline{\nu_N}=\frac{1}{2}$, because the long-range order of the stripe phase is destroyed by disorder. This explains narrow peaks of σ_{xx} at zero temperature at half-integer ν's.

At nonzero temperature the peaks have a finite width due to a hopping between spatially close $\nu_N=1$ domains. However, the consideration of such a hopping goes beyond the scope of the present paper.

The outline of the paper is as follows. In Sec. II we present a qualitative discussion where we show that even a perfectly repulsive interaction may cause the clusterization of particles. In Sec. III we formulate the self-consistent HF problem and give its approximate solution under two kinds of simplifying assumptions (one corresponds to ''stripes'' and the other to ''bubbles''). In Sec. IV we report the results of a numerical study of CDW patterns based on the trial wave function (3). In Sec. V we discuss the implications of the CDW state for the double-well tunneling experiments. Finally, Sec. VI is devoted to conclusions. Various details of calculations, e.g., a careful comparison of the energies of the CDW and the conventional WC, may be found in the Appendixes.

II. QUALITATIVE DISCUSSION

Our results can be understood by analyzing the following toy model. Consider a one-dimensional (1D) lattice gas interacting via the boxlike potential

$$u(x)=u_0\Theta(2R-|x|) \qquad (6)$$

and situated on the background of the same average density, interaction with which is described by the potential of the same type but with the opposite sign. One can say that each particle has a negative unit charge while the background is charged positively. We assume that R is much larger than the lattice constant a. We also assume that a multiple occupancy of the sites is forbidden; then the average occupancy or the average filling factor $\overline{\nu}$ is always between 1 and 0. Let us focus on the case $\overline{\nu}=\frac{1}{2}$.

One of the possible particle distributions is the WC, i.e., the state where every other lattice site is occupied. It can be shown that the absolute value of its cohesive energy does not exceed u_0, the maximum value of the two-particle interaction potential. Now we demonstrate that at $\overline{\nu}=1/2$ the arrangement of the particles in a series of equidistant large clusters of width $\sim R$ allows the system to attain the cohesive energy as small as

$$E_{\rm coh}=-(3-2\sqrt{2})(R/a)u_0. \qquad (7)$$

For the obvious reason we call this state the CDW state. Since the spatial period $\Lambda\sim R$ of this state is much larger

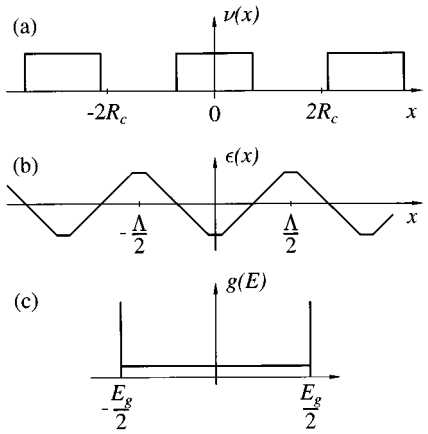

FIG. 3. The CDW in the lattice gas. (a) Local filling factor $\nu(x)$. (b) One-particle energy $\epsilon(x)$. (c) DOS in the lattice gas.

than the average interparticle distance, it is convenient to switch from the description in terms of discrete particles to the continual representation where one uses the local filling factor $\nu(x)$. We consider the CDW with the boxlike profile of $\nu(x)$:

$$\nu(x)=\Theta\left(\frac{\Lambda}{4}-|x|\right), \quad -\frac{\Lambda}{2}<x<\frac{\Lambda}{2}; \tag{8}$$

see Fig. 3(a). The lowest value of the energy quoted above is reached at $\Lambda=2\sqrt{2}R\approx 2.8R$. Indeed, this period is much larger than the average interparticle distance $2a$, i.e., instead of being equidistant as in the WC, the particles are compacted in large clusters of the highest possible density a^{-1}.

The clusterization is advantageous because in contrast to, e.g., the usual Coulomb law, here the interaction potential ceases to increase at distances smaller than $2R$. Therefore, particles can be brought closer to each other at no energy cost. At the same time the particles in the interior of a given cluster avoid the particles in the other clusters. Hence, they interact only with the charge $\Lambda/2a$ of their own cluster. Now recall that each particle interacts with the background as well. The amount of the background charge involved in this interaction is $(2R/a)>(\Lambda/2a)$. Therefore, the interaction with the positive background dominates and each cluster resides in a deep potential well. The cohesive energy of the system is determined simply by the average depth of this well. Let us now calculate the cohesive energy and then minimize it with respect to Λ. This way we will find the optimal period of the state.

Define the one-particle energy $\epsilon(x)$ at a point x by

$$\epsilon(x)=\int \frac{dx'}{a}u(x-x')[\nu(x')-\overline{\nu}], \tag{9}$$

then the cohesive energy is determined by the average value of $\epsilon(x)\nu(x)$:

$$E_{\rm coh}=\frac{1}{2\overline{\nu}}\langle\epsilon(x)\nu(x)\rangle. \tag{10}$$

It is easy to see that for $\nu(x)$ given by Eq. (8) and Λ in the range $\frac{8}{3}R<\Lambda<4R$, $\epsilon(x)$ has an approximately sawtooth form [Fig. 3(b)] and oscillates between $\pm\frac{1}{2}E_g$, where

$$E_g=u_0\frac{4R-\Lambda}{a}. \tag{11}$$

The cohesive energy can be readily evaluated to be $E_{\rm coh}(\Lambda)=-E_g(\Lambda-2R)/2\Lambda$, which reaches its lowest value (7) at $\Lambda=2\sqrt{2}R$.

Let us now calculate the DOS $g(E)$, which we define by

$$g(E)=\frac{1}{L_x}\int dx\,\delta(\epsilon(x)-E), \tag{12}$$

where L_x is the length of the system. The integration yields

$$g(E)=\frac{2}{\Lambda}\begin{cases}\left|\dfrac{d\epsilon}{dx}\right|^{-1}, & |E|<\frac{1}{2}E_g\\ 0, & |E|>\frac{1}{2}E_g,\end{cases} \tag{13}$$

where the coordinate x appearing on the upper line of Eq. (13) is any of those where $\epsilon(x)=E$. Clearly, $g(E)$ is constant in the interval $-\frac{1}{2}E_g<E<\frac{1}{2}E_g$ but diverges at the end points of this interval [Fig. 3(c)]. These divergencies are the particular form of the Van Hove singularities inherent to the DOS of all periodic structures.

Let us now return from the toy model to the real electrons at the upper partially filled LL. Consider again the case $\overline{\nu_N}=\frac{1}{2}$. As discussed in Sec. I, at such $\overline{\nu_N}$ the stripe CDW pattern forms. In this case the problem is effectively 1D because the one-electron basis states can be chosen in such a way that they are labeled by one quantum number (the guiding center coordinate) X. In the Landau gauge $\boldsymbol{A}=-Bx\hat{\boldsymbol{y}}$, the wave function of one of such states is given by

$$\psi_X=\frac{e^{iyX/l^2}}{\pi^{1/4}\sqrt{2^N N! l L_y}}\exp\left[-\frac{(x-X)^2}{2l^2}\right]H_N\left(\frac{x-X}{l}\right), \tag{14}$$

where L_y is the y dimension of the system and $H_N(x)$ is the Hermite polynomial.[25] The wave function (14) is extended in the y direction but has a finite spread of $2R_c$ in the x direction. Strictly speaking, the HF potential $u_{\rm HF}(x)$ via which the basis states interact, is different from the one given by Eq. (6). However, as will be shown in the next section, for $r_s\sim 1$ this potential is roughly equivalent to

$$u_{\rm HF}^{\rm eff}(x)=a\frac{\hbar\omega_c}{2\pi^2 R_c}\Theta(2R_c-|x|)-aE_h\delta(x), \tag{15}$$

$$a=\frac{2\pi l^2}{L_y}. \tag{16}$$

Such a formula for $u_{\rm HF}^{\rm eff}(x)$ results from the particular form of the bare interaction potential $v(r)$ (the interaction potential of two pointlike charges) in the 2DEG in a weak magnetic field, which is as follows. At very short $r\ll a_B$ and very large $r\gg R_c^2/a_B$ distances, $v(r)$ coincides with the usual Coulomb law $v(r)=e^2/\kappa r$. At intermediate distances, it is significantly smaller than the Coulomb potential because of a

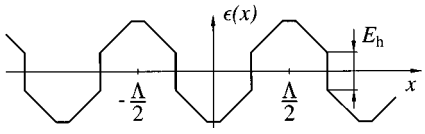

FIG. 4. One-particle energy $\epsilon(x)$ for the CDW in the real system (schematically).

strong screening by the large number of electrons at the lower LL's. Very crudely, $v(r)$ can be approximated by

$$v(\boldsymbol{r}) = \pi e^2 a_B \delta(\boldsymbol{r}) + E_h, \quad r \lesssim 2R_c, \tag{17}$$

where $E_h = (e^2 a_B/\kappa R_c^2)\ln(R_c/\sqrt{2}a_B)$ [cf. Eq. (2)].

Clearly, the first term in $v(r)$ gives a nonvanishing contribution to the interaction potential $u_{\rm HF}(x)$ between two basis states only if the densities of the two states overlap, i.e., at $|x| < 2R_c$. Beyond $2R_c$, this contribution becomes very small. This is represented by the first term in Eq. (15), which exhibits a steplike discontinuity at $|x| = 2R_c$.

The second term in $u_{\rm HF}^{\rm eff}(x)$ comes from the second (''hydrodynamic'') term in the bare interaction potential. It is important that this second term in $v(r)$ is almost constant in real space up to rather large distances (of the order of several R_c). It is then clear on physical grounds that this long-range ''hydrodynamic'' term in $v(r)$ [or its image $aE_h\delta(x)$ in $u_{\rm HF}^{\rm eff}$] has no effect on the short length scale structure of the ground state. In other words, as long as the characteristic spatial scales of a given state are of the order of R_c or shorter, the contribution of the ''hydrodynamic'' term to the cohesive energy of such a state is the same. It can be shown that this contribution is equal to

$$E_{\rm coh}^h = -\frac{1-\overline{\nu_N}}{2} E_h \tag{18}$$

(see also Sec. III). Therefore, the ground-state structure is determined by the boxlike part and is exactly the same as in our toy model [see Fig. 3(a)].

Given the results of the toy model, we can immediately derive the quantities of interest for the real system (in the practically important case $r_s \sim 1$) as well. First, the optimal CDW period Λ should be close to $2.8R_c$. Indeed, we found the value of $2.7R_c$ for this quantity. Second, Eq. (4) for the cohesive energy follows from Eq. (7) after the appropriate substitutions for u_0 and R by the parameters from Eq. (15). [One should not forget here to add the contribution of the short-range part given by Eq. (18)]. Finally, to deduce the functional form of the DOS, let us examine the effect of this short-range part on $\epsilon(x)$. Clearly, it is to lower $\epsilon(x)$ by $\frac{1}{2}E_h$ in $\nu(x)=1$ intervals and to raise it by the same amount in the other intervals where $\nu(x)=0$. This generates the jumps in $\epsilon(x)$ at $x = \pm\frac{1}{4}\Lambda$ (Fig. 4) superimposed on the familiar sawtooth profile of $\epsilon(x)$ in the lattice gas model [Fig. 3(b)]. Hence, the effect of the short-range part on the DOS is to insert a hard gap of width E_h centered at zero energy (Fig. 2). Therefore, E_g is augmented by the same value, which is accounted for by the second term in Eq. (5). The first term in this equation (for $r_s \sim 1$) follows from Eq. (11) upon the appropriate substitutions for u_0 and R.

Note that in the real system, unlike in the toy model, the Van Hove singularities at the edges of the spectrum are not δ-function-like but the inverse square-root ones. Indeed, the DOS is inversely proportional to $d\epsilon/dx$; hence, the type of singularity at, say, $E = -\frac{1}{2}E_g$ is determined by how this derivative goes to zero at $x \to 0$. The real interaction potential is never an ideally flat-top box, and in reality the extrema in $\epsilon(x)$ in Fig. 2 are, in fact, somewhat rounded. We expect that the second derivative $d^2\epsilon/dx^2$ is finite at $x=0$, which corresponds to the inverse square-root singularity in $g(E)$.

Our toy model enabled us to derive our main results [Eqs. (4,5)] for the most practical case of $r_s \sim 1$. At smaller r_s the potential is no longer boxlike and we have to examine the problem more carefully, which will be done in the next section. Before we do so, it is important to identify a general criterion, which enables one to tell whether or not a given type of the repulsive interaction would lead to a similar clusterization of particles. This criterion can be obtained by analyzing the Fourier transform of the potential and it is well known in the theory of the CDW systems.

For simplicity, let us return to the 1D case. The cohesive energy can be written as

$$E_{\rm coh} = \frac{1}{2L_x \overline{\nu}\overline{a}^2} \sum_{q \neq 0} \tilde{u}(q)\tilde{\nu}^2(q), \tag{19}$$

where L_x is the length of the system. (From now on, where using the same symbol for both real-space and q-space quantities may lead to an ambiguity, the Fourier transformed quantities are denoted by tildes.) Obviously, if $\tilde{u}(q)$ is negative at a certain q, then the formation of a CDW with such q will lead to the lowering of the system energy. Therefore, the criterion for the CDW instability is the presence of *negative values* of $\tilde{u}(q)$. The Fourier transform of the boxlike potential (6) is given by $\tilde{u}(q) = 2\sin(2qR)/q$, which is indeed negative at certain q. Note also that the CDW instability is the strongest at $q = 3\pi/4R$ where $\tilde{u}(q)$ reaches its lowest value. This particular q corresponds to the spatial period of $\frac{8}{3}R \approx 2.67R$, which is very close to the optimal period of approximately $2.8R$ we found above. The reason why they are slightly different is that the CDW instability enters the nonlinear regime. Apparently, a small change in the period enables the CDW to incorporate the contribution of subleading harmonics in a more optimal way.

In the next section we give details of the HF approximation from which the true form of the interaction potential can be found.

III. CDW STATE

In this section we formulate the self-consistent HF problem and give its approximate solution.

The first-principles formulation of the HF problem takes into consideration all occupied $N+1$ LL's together with several low-lying empty ones. In other words, it deals with $O(N)$ different species of fermions interacting via $O(N^2)$ different types of interactions among themselves. Although for moderate N such a treatment is feasible, the solution can be obtained only numerically (see, e.g., MacDonald and Aers[26]).

A different approach was put forward by Aleiner and

Glazman.[9] They showed that at sufficiently large N, $N \gg r_s^{-1} \gg 1$, the degrees of freedom associated with lower N LL's can be integrated out, and derived an effective Hamiltonian[9] governing the low-energy physics of the 2D liquid in a weak magnetic field:

$$\hat{H}_{\rm eff} = \frac{1}{2L_xL_y} \sum_{\boldsymbol{q}} \rho(\boldsymbol{q}) \tilde{v}(\boldsymbol{q}) \rho(-\boldsymbol{q}), \tag{20}$$

where $\rho(\boldsymbol{q})$ is the projection of the density operator onto the upper LL and

$$\tilde{\nu}(q) = \frac{2\pi e^2}{\varepsilon(q) q} \tag{21}$$

is the renormalized interaction potential (recall that the tilde is used for Fourier transformed quantities). Physically, the bare Coulomb interaction among the electrons at the upper partially filled LL gets renormalized because electric fields become screened by the lower completely filled LL's. The quantity $\varepsilon(q)$ has, therefore, the meaning of the dielectric constant for the system of the filled LL's. It is given by[9]

$$\varepsilon(q) = \kappa \left\{ 1 + \frac{2}{q a_B} [1 - J_0^2(qR_c)] \right\}, \tag{22}$$

where κ is the background dielectric constant and J_0 is the Bessel function of the first kind.[25] Note that the asymptotic expressions for $\varepsilon(q)$,

$$\varepsilon(q) = \kappa \begin{cases} 1 + \dfrac{2}{q a_B}, & R_c^{-1} \ll q \ll k_F \\ 1 + \dfrac{R_c^2 q}{a_B}, & q \ll R_c^{-1}, \end{cases} \tag{23}$$

were obtained earlier by Kukushkin, Meshkov, and Timofeev.[27] Equation (17) of Sec. II can be obtained by performing the Fourier transform of Eq. (21).

Let us return to Eq. (20). It contains the density operator $\rho(\boldsymbol{q})$ projected on the upper LL expressible in the form

$$\rho(\boldsymbol{q}) = \sum_X F(q) e^{-iq_x X} a^\dagger_{X_+} a_{X_-}, \tag{24}$$

where $a^\dagger_X$ (a_X) is the creation (annihilation) operator of the state (14), $X_\pm$ are defined by $X_\pm = X \pm q_y l^2/2$, and $F(q)$, given by

$$F(q) = \int dx\, dy |\psi_X|^2 e^{-iqx}, \tag{25}$$

bares the name of the form factor of state (14). Performing the integration, one obtains

$$F(q) = \exp\left(-\frac{q^2 l^2}{4} \right) L_N\left(\frac{q^2 l^2}{2} \right), \tag{26}$$

$L_N(x)$ being the Laguerre polynomial.[25] Following the usual procedure of the HF decoupling of the Hamiltonian (20) we get

$$\hat{H}_{\rm HF} = \frac{n_L}{2} \sum_{\boldsymbol{q}} \tilde{u}_{\rm HF}(\boldsymbol{q}) \Delta(-\boldsymbol{q}) \sum_X e^{-iq_x X} a^\dagger_{X_+} a_{X_-}, \tag{27}$$

where $n_L = (2\pi l^2)^{-1}$ is the density of one completely filled LL and

$$\Delta(\boldsymbol{q}) = \frac{2\pi l^2}{L_x L_y} \sum_X e^{-iq_x X} \langle a^\dagger_{X_+} a_{X_-} \rangle \tag{28}$$

is the CDW order parameter.[2,3] By $\tilde{u}_{\rm HF}$ in Eq. (27) we denote the HF potential, $\tilde{u}_{\rm HF}(q) = \tilde{u}_{\rm H}(q) - \tilde{u}_{\rm ex}(q)$. The Hartree potential $\tilde{u}_{\rm H}(q)$ is given by

$$\tilde{u}_{\rm H}(q) = \tilde{v}(q) F^2(q). \tag{29}$$

The exchange potential $\tilde{u}_{\rm ex}(q)$ in the reciprocal space turns out to be proportional to the real-space Hartree potential,

$$\tilde{u}_{\rm ex}(q) = u_{\rm H}(ql^2)/n_L. \tag{30}$$

From Eqs. (26), (29), and (30) and also from an asymptotic formula for $F(q)$,

$$F(q) \simeq J_0(qR_c), \quad q \ll k_F, \tag{31}$$

more convenient expressions for $\tilde{u}_{\rm H}(q)$ and $\tilde{u}_{\rm ex}(q)$ at $R_c^{-1} \lesssim q \ll k_{\rm F}$ can be derived:

$$n_L \tilde{u}_H(q) \approx \frac{\hbar\omega_c}{2 + q a_B} J_0^2(qR_c), \tag{32}$$

$$n_L \tilde{u}_{\rm ex}(q) \approx \frac{r_s \hbar\omega_c}{\sqrt{2}\pi} \left\{ \ln\left(1 + \frac{r_s^{-1}}{\sqrt{2} q R_c} \right) + \frac{\sin(2qR_c)}{2qR_c[1 + (r_s/\sqrt{2})]} \right\} + E_h. \tag{33}$$

The cohesive energy can be obtained from Eq. (27) by omitting the wave vector $q = 0$ in the sum, taking the quantum-mechanical average, and then dividing the result by the total number of particles $\overline{\nu_N} n_L L_x L_y$ at the upper LL, which gives

$$E_{\rm coh} = \frac{n_{\rm L}}{2\overline{\nu_N}} \sum_{\boldsymbol{q} \neq 0} \tilde{u}_{\rm HF}(q) |\Delta(\boldsymbol{q})|^2. \tag{34}$$

We want to find the set of the CDW order parameters $\Delta(\boldsymbol{q})$ that minimizes the cohesive energy under certain conditions of the self-consistency (see below) imposed on $\Delta(\boldsymbol{q})$. We will present an approximate solution based on the consideration of only two idealized CDW patterns: a system of uniform parallel stripes and a triangular lattice of perfectly round ''bubbles.'' As mentioned in the Introduction, the stripe phase is more favorable in some interval of $\overline{\nu_N}$ around half filling. Outside of this interval, it gets replaced by the ''bubble'' phase. We will consider the two phases separately.

A. Stripe phase

In this case $\Delta(\boldsymbol{q})$ are nonzero only if $q_y = 0$. It is convenient to introduce the local filling factor ν_N (compare with $\overline{\nu_N}$, the *average* filling factor) by $\nu_N(x,y) = \nu_N(x) \equiv \langle a_x^\dagger a_x \rangle$. In the stripe phase, the order parameter Δ and ν_N are just proportional to each other:

$$\Delta = \frac{\nu_N}{L_x L_y}. \tag{35}$$

The self-consistency condition mentioned above is

$$\nu_N(x)=\Theta[\epsilon_F-\epsilon(x)], \tag{36}$$

whose meaning is that all the states below the Fermi level ϵ_F are filled, and all others are empty. The self-consistent potential $\epsilon(x)$ in Eq. (36) is given by

$$\epsilon(x)=n_L\sum_{q\neq 0}\tilde{u}_{\rm HF}(q)\Delta(q\hat{\mathbf{x}})e^{iqx}. \tag{37}$$

By $\hat{\mathbf{x}}$ we mean the unit vector in the x direction. Equations (34)–(37) define the HF problem for the case of the unidirectional CDW.

For $N>0$ the Hartree potential $\tilde{u}_H(q)$ inevitably has zeros due to the factor $F(q)$ containing the Laguerre polynomial [Eq. (29)]. The first zero, q_0, is approximately given by $q_0\approx 2.4/R_c$. Since the exchange potential is always positive [Eq. (33)], there exist q's where the total HF potential $\tilde{u}_{\rm HF}$ is negative. This leads to the CDW instability because the energy can be reduced by creating a perturbation at any of such wave vectors (cf. Ref. 2).

We will focus on the parameter range $0.06<r_s<1$ and $N<50$, which covers the cases of the experimental practice and even beyond that. In such a parameter range, the HF potential is negative at all wave vectors $q>q_0$ and reaches its lowest value near $q=q_0$ (see Fig. 2 of Ref. 6). One can guess then that the lowest-energy CDW is the one with the largest possible [under the conditions (36) and (37)] value of $|\Delta(q_0\hat{\mathbf{x}})|$. The CDW having this property consists of alternating stripes with filling factors $\nu_N(x)=0$ and $=1$ [Fig. 1(b)]. Within the class of unidirectional CDW's we are considering now, this guess turns out to be correct. However, due to the anharmonism of such a solution, the optimal spatial period Λ of the CDW is slightly larger than $2\pi/q_0$ and is equal to

$$\Lambda=2.7R_c. \tag{38}$$

Nonzero $\Delta(\boldsymbol{q})$ for this solution are given by

$$\Delta(q\hat{\mathbf{x}})=\frac{2}{\Lambda q}\sin\left(\frac{\overline{\nu_N}}{2}\Lambda q\right) \tag{39}$$

provided q is an integer multiple of $2\pi/\Lambda$.

Let us now derive Eq. (5) for the pseudogap. Clearly, $E_g=2|\epsilon(0)|$. To calculate $\epsilon(0)$ we could, in principle, use Eqs. (32) and (33) to sum the series in Eq. (37). However, to establish the connection with Sec. II, we will switch to real space. Define a 1D HF potential,

$$u_{\rm HF}(x)\equiv\frac{1}{L_y}\int dq e^{iqx}\tilde{u}_{\rm HF}(q), \tag{40}$$

then $\epsilon(x)$ will be related to $\nu_N(x)$ in a way similar to Eq. (9):

$$\epsilon(x)=\int\frac{dx'}{a}u_{\rm HF}(x-x')[\nu_N(x')-\overline{\nu_N}], \tag{41}$$

where a is given by Eq. (16).

At large N the potential $u_{\rm HF}(x)$ can be approximated by

$$u_{\rm HF}^{\rm eff}(x)=a\frac{\hbar\omega_c}{2\pi^2 R}B(x)-aE_h\delta(x), \tag{42}$$

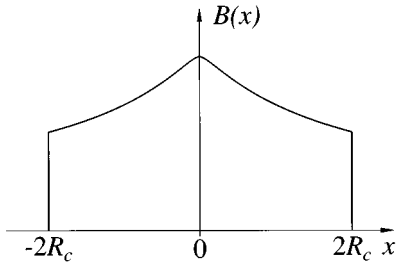

FIG. 5. The function $B(x)$.

$$B(x)=\int_0^{\pi/2}\frac{d\varphi}{(r_s/\sqrt{2})+\sqrt{1-[1-k^2(x)]\sin^2\varphi}}, \tag{43}$$

where $k(x)\equiv x/2R_c$ (see Appendix A). Equation (42) is a good approximation if one is not interested in the detailed behavior of $u_{\rm HF}(x)$ at x smaller than a_B or larger than several R_c. For $r_s\ll 1$ the function $B(x)$ satisfies the following asymptotic relations:

$$B(x)=\begin{cases}\ln\left(\dfrac{2\sqrt{2}}{r_s}\right), & x=0\\ K'\left(\dfrac{x}{2R_c}\right), & r_sR_c\lesssim|x|<2R_c\\ 0, & |x|>2R_c,\end{cases} \tag{44}$$

where K' is the complete elliptic integral of the first kind.[25] The plot of $B(x)$ is shown schematically in Fig. 5. One can see that it has a steplike discontinuity at $x=2R_c$ already mentioned in Sec. II. In fact, at $r_s\sim 1$, $B(x)$ is very nearly boxlike, $B(x)\sim\Theta(2R_c-|x|)$ and Eq. (15) follows.

Using Eqs. (41) and (42), we find for E_g:

$$E_g=\frac{\hbar\omega_c}{\pi^2 R_c}\int_0^{2R_c}dxB(x)\,\mathrm{sgn}\left(x-\frac{\Lambda}{4}\right)+E_h, \tag{45}$$

which with the help of Eq. (43) can be transformed into

$$E_g\approx\hbar\omega_c\left(0.013+\frac{r_s}{\sqrt{2}\pi}\int_{r_s}^{\Lambda/8R_c}\frac{dk}{k}\right)+E_h. \tag{46}$$

After the substitution $\Lambda=2.7R_c$, one recovers Eq. (5). [The small number in the parentheses of Eq. (46) is the result of a numerical evaluation of a certain integral. To obtain Eq. (5) it was disregarded.]

Let us now calculate the cohesive energy [Eq. (4)]. When r_s is not much smaller than unity, $B(x)$ remains approximately boxlike, and, consequently, $\epsilon(x)$ in the $\nu_N(x)=1$ intervals has an essentially triangular cusp (Fig. 4). Using Eq. (10), we then arrive at

$$E_{\rm coh}^{\rm CDW}=-\tfrac{1}{8}(E_g+E_h), \tag{47}$$

which leads to Eq. (4).

Note that at smaller r_s, $r_s\sim 0.1$, the cusp in $\epsilon(x)$ deviates from the triangular form. This is illustrated in Fig. 6, where $\epsilon(x)$ for $r_s=0.1$, $N=30$ is shown. In this figure one can see the bending of the initially straight lines of Fig. 4.

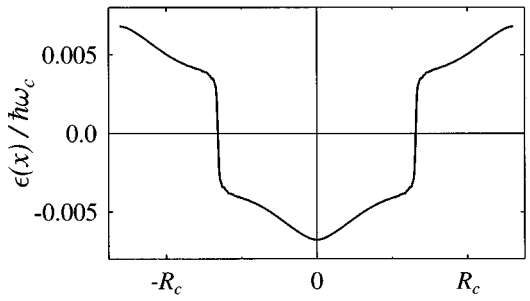

FIG. 6. $\epsilon(x)$ for $r_s=0.1$, $N=30$.

This bending is due to the deviation of $B(x)$ from the ideally flat-top box, or in physical terms, due to the Hartree term in the interaction. The Hartree interaction reduces the slope of $\epsilon(x)$, or the magnitude of the directed inward the stripes ''electric field'' $-(d\epsilon/dx)\hat{\boldsymbol{x}}$. The magnitude of the field is equal to

$$\frac{d\epsilon}{dx}=\frac{\hbar\omega_c}{2\pi^2 R_c}\left[2B\left(\frac{\Lambda}{2}\right)-B(0)\right]. \tag{48}$$

at the stripe boundary $x=\Lambda/4$ (or, more precisely, at a distance $\sim a_B$ from the boundary). Equation (48) enables one to find the range of r_s where the simple CDW profile with one stripe per period remains stable. Indeed, there is a critical value of r_s at which the electric field near the stripe boundary vanishes. Using Eqs. (38), (44), and (48), one arrives at

$$r_s^*=2\sqrt{2}\exp\left[-2K'\left(\frac{\Lambda}{4R_c}\right)\right]\approx 0.06 \tag{49}$$

for the critical r_s. At $r_s=r_s^*$, the original stripe breaks into three smaller ones: the central one, almost as wide as the original stripe, and two narrow ones (of width $\sim a_B$) on the sides [Fig. 7(b)]. Note that this transformation resembles the edge reconstruction of quantum dots[28] (the decrease of r_s in this analogy is equivalent to the steepening of the quantum dot confining potential).

Since $r_s=0.06$ is rather difficult to reach under the terrestrial conditions, only the boxlike solution and Eq. (4) have a practical value. The next four paragraphs are devoted to a purely theoretical issue of the CDW structure at truly small r_s. Uninterested readers can skip these paragraphs.

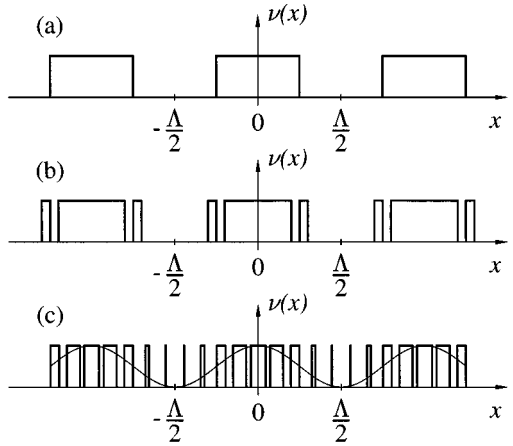

FIG. 7. The local filling factor in the stripe CDW pattern for different r_s. (a) $r_s>r_s^*$, (b) $r_s\sim r_s^*$, (c) $r_s\ll r_s^*$.

We expect that the reduction of r_s beyond r_s^* leads to a further increase in the number of stripes per period. It is important also that these stripes will be of unequal width, such that after a coarse-grain averaging of the filling factor $\nu_N(x)$, it would appear approximately sinusoidal [Fig. 7(c)]. To understand this let us go back to the q space.

In the limit $r_s\ll r_s^*$ and $N\gg r_s^{-2}$, the exchange potential $\tilde{u}_{\rm ex}(q)$ is on average much smaller than the Hartree potential $\tilde{u}_{\rm H}(q)$ for $R_c^{-1}<q<(R_c r_s)^{-1}$ [see Eqs. (29) and (33)], so the total HF potential is negative in small q intervals centered at the zeros of $\tilde{u}_{\rm H}(q)$. The absolute minimum of $\tilde{u}_{\rm HF}(q)$ is still situated near $q=q_0$. If one chooses the wave vector of the principle harmonic to be q_0, already the next harmonic of the boxlike profile $q=3q_0$ will correspond to a large positive $\tilde{u}_{\rm HF}(q)$. Hence, to minimize the energy of the system all such unfavorable harmonics must be suppressed. In other words, the CDW may be only slightly anharmonic. In a simplified description, the spatial distribution of the filling factor is sinusoidal, and has the amplitude $\overline{\nu_N}$ and the spatial period $2\pi/q_0$. Let us find the cohesive energy of the stripe phase at given $\overline{\nu_N}$. Since the filling factor is approximately sinusoidal in x, in formula (34) we have to retain only two terms with $q_x=\pm q_0$ for which $|\Delta(\boldsymbol{q})|\simeq\frac{1}{2}\overline{\nu_N}$. Taking advantage of Eq. (33), we arrive at the estimate

$$E_{\rm coh}^{\rm CDW}\simeq-\frac{\overline{\nu_N}r_s\hbar\omega_c}{4\sqrt{2}\pi}\ln\left(1+\frac{0.3}{r_s}\right)-\frac{1-\overline{\nu_N}}{2}E_h. \tag{50}$$

The last term was obtained by a more accurate procedure based on the sum rule[3]

$$\sum_{\boldsymbol{q}\neq 0}|\Delta(\boldsymbol{q})|^2=\overline{\nu_N}(1-\overline{\nu_N}), \tag{51}$$

which is just another way to derive Eq. (18).

In fact, the function $\nu_N(x)$ is more complicated. First, there are deviations from the pure sinusoidal form in narrow regions centered at the extrema of $\nu_N(x)$. In these regions $\nu_N(x)$ is flattened, such that it reaches zero (or one) not at single points but in small intervals of x. Second, even with these corrections, the simple sinusoidal of $\nu_N(x)$ is not the complete answer yet because, taken literally, it contradicts Eq. (36). Indeed, according to Eq. (36), the local filling factor can be only one or zero whereas we just argued that $\nu_N(x)$ takes intermediate values as well. The contradiction is resolved by the fine structure of the CDW. Namely, the CDW profile consists of many narrow boxes [Fig. 7(c)], and appears sinusoidal only after the coarse-grain averaging. To find the characteristic width of such boxes we have to analyze the HF potential more carefully. It is easy to see that at wave vectors $q>1/R_c r_s$, the exchange potential becomes larger than the average of the oscillating Hartree potential [Eqs. (29) and (33)]. Therefore, in this range of q there are many harmonics, which need not be suppressed. Thus, the typical distance between the boxes is of the order of $\xi\equiv\sqrt{2}r_s R_c$. The appearance of the scale ξ in the ground-state structure is not accidental. It is related to the fact that

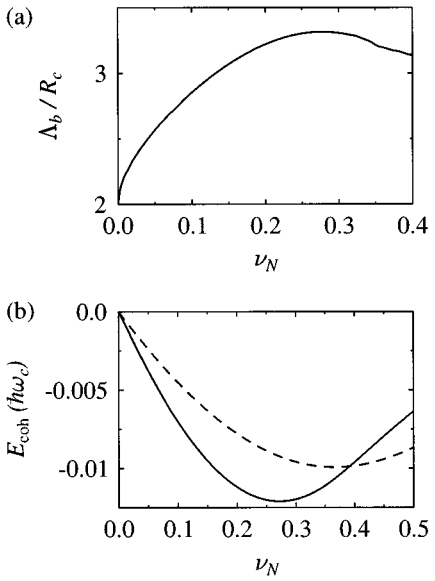

FIG. 8. (a) The optimal distance Λ_b between neighboring bubbles as a function of the filling factor. (b) The cohesive energy of the ''bubble'' and stripe phases (solid and dashed lines, respectively). The plotted dependencies correspond to the limit $N\to\infty$, $r_s\sim 1$. The ''hydrodynamic'' term in the cohesive energy, small in this limit, is neglected.

ξ is nothing more than the range of the exchange potential $u_{\rm ex}(r)$ in real space [at $r>\xi$ $u_{\rm ex}(r)$ rapidly decreases: $u_{\rm ex}(r)\propto 1/r^2$].

B. ''Bubble'' phase

We will consider only the large-N limit where $R_c\gg l$ and, therefore, both the period of the bubble lattice and the radius of the ''bubbles'' are much larger than the magnetic length. In this case we can still use the concept of the local filling factor, but now it depends on both x and y coordinates. The filling factor $\nu_N(x,y)$ is assumed to be unity inside the ''bubbles'' and zero everywhere else. The ''bubbles'' form a triangular lattice. The relation between the lattice constant Λ_b and the radius r_b of the ''bubbles'' is

$$\frac{r_b}{\Lambda_b}=\left(\frac{\sqrt{3}\overline{\nu_N}}{2\pi}\right)^{1/2}. \tag{52}$$

Similar to the case of stripes, we will use an asymptotic expression for the HF potential,

$$n_L u_{\rm HF}(\boldsymbol{r})\approx\frac{\hbar\omega_c}{2\pi^3 R_c}\frac{\Theta(2R_c-r)}{\sqrt{4R_c^2-r^2}}+E_h[n_L-\delta(\boldsymbol{r})], \tag{53}$$

valid at $r_s\sim 1$ and r smaller than several R_c. One possible way to obtain this equation is to start from the formula for $u_{\rm HF}^{\rm eff}$ in q space (see Sec. II) and then perform its 2D Fourier transform.

With the help of Eqs. (52) and (53), for every given $\overline{\nu_N}$ we have numerically calculated the cohesive energy of the ''bubble'' phase as a function of Λ_b. This way we have been able to determine the optimal value of Λ_b, which is plotted in Fig. 8(a). Note that at $\nu_N\lesssim 0.1$ the optimal period closely follows the formula

$$\Lambda_b\simeq\frac{2R_c}{1-2(r_b/\Lambda_b)}, \tag{54}$$

whose meaning is that the neighboring ''bubbles'' barely interact with each other.

At $\overline{\nu_N}=\nu_N^*\approx 0.39$, the cohesive energies of the stripe and the ''bubble'' phases become equal [Fig. 8(b)]. At smaller $\overline{\nu_N}$, the ''bubble'' phase replaces the ''stripes.'' Arguments can be given that this transition is of first order.[29]

The dominance of the ''bubble'' phase over the ''stripes'' at small $\overline{\nu_N}$ allows a simple geometrical interpretation. Recall that at small $\overline{\nu_N}$ the ''bubbles'' barely interact with each other. The situation in the stripe phase is similar: the optimal period is very close to $\Lambda\simeq 2R_c/(1-\overline{\nu_N})$, so that only the particles within the same stripe interact with each other. Given this, the cohesive energy is determined by the interactions of particles within a single stripe (for the stripe phase) or within a single ''bubble'' (for the ''bubble'' phase). In the stripe phase, each particle interacts with all the particles within the area $4R_c\times\Lambda\,\overline{\nu_N}\simeq 8R_c^2\overline{\nu_N}$. In the ''bubble'' phase, the corresponding area is $\pi r_b^2\simeq 2\sqrt{3}R_c^2\overline{\nu_N}$, i.e., roughly a factor of 2 smaller. Thus, in the ''bubble'' phase the particles avoid each other more effectively, and this phase should be more energetically favorable. It is possible to further elaborate upon this way of reasoning and to show that for the interaction potential (53), the ratio of the cohesive energies of the two phases tends to 1.7 as $\overline{\nu_N}\to 0$ in agreement with data of Fig. 8(b).

On the intuitive level, the ''bubble'' phase is expected to appear as ν_N decreases because of the imminent Wigner crystallization at sufficiently small $\overline{\nu_N}$. Indeed, the WC is a particular case of the ''bubble'' phase with $n_e=1$, where n_e is the number of particles in one ''bubble.'' When $\overline{\nu_N}\gg 1/N$, n_e is large and can be found from

$$n_e=\frac{\sqrt{3}}{2\pi}\left(\frac{\Lambda_b}{R_c}\right)^2 N\overline{\nu_N}. \tag{55}$$

following from Eq. (52). As $\overline{\nu_N}$ becomes smaller, n_e decreases. Eventually, at $\overline{\nu_N}\sim 1/N$, n_e reaches the value of one and the ''bubble'' state becomes the ordinary WC. Thus, the ''bubble'' phase appears as a natural intermediate state between the stripe phase and the WC.

Equation (55) implies that in the interval $1/N<\overline{\nu_N}\leqslant\frac{1}{2}$ the optimal number of electrons in one ''bubble'' is larger than one; i.e., the ''bubble'' phase is more energetically favorable than the WC. This issue is discussed in more detail in Appendix B.

So far, we have been discussing the case $r_s\sim 1$. We expect that with decreasing r_s, the original ''bubbles'' break into smaller ones, similar to the case of the stripes [Figs. 7(b) and 7(c)]. The characteristic distance between neighboring bubbles is of the order of $\xi\sim\Lambda r_s$. Such smaller ''bubbles'' contain fewer electrons each; therefore, the transition to the WC phase occurs at larger filling factor $\overline{\nu_N}\sim 1/(Nr_s^2)$.

Section IV is devoted to numerical simulations, which confirm the formation of the stripe and ''bubble'' phases.

IV. NUMERICAL STUDY

In Sec. III we showed that the electron liquid at the upper partially filled LL is unstable against the CDW formation. At not too small (''realistic'') r_s, the CDW instability is rather strong and it causes the uniform electron liquid to break into occupied and empty domains (Fig. 1). It is difficult to find the optimal shape of such domains analytically,[15] and to study this question we resorted to numerical simulations, described below.

The trial wave function used in our finite-size modeling is given by Eq. (3) where the centers $\boldsymbol{R}_i$ are chosen from the sites of the triangular lattice. The lattice constant is equal to $(4\pi/\sqrt{3})^{1/2}l$ in physical units. Hence, the fully populated lattice corresponds to the average density $1/(2\pi l^2)$, i.e., to the filling factor $\overline{\nu_N}=1$. Denote by $n_i \in \{0,1\}$ the occupancy of the ith site. Let us derive the expression for the cohesive energy of the trial state in terms of n_i.

We begin by examining a state with a single occupied site at the origin. This state bares the name of the coherent state.[13] The following properties of such a state are important for us. First, the probability density distribution, i.e., the square of the absolute value of the wave function $\phi(\boldsymbol{r})$ of the coherent state is given by

$$|\phi(\boldsymbol{r})|^2=\frac{1}{2\pi l^2 N!}\left(\frac{r^2}{2l^2}\right)^N e^{-r^2/2l^2}. \tag{56}$$

It has a sharp maximum at $r=\sqrt{2N+1}\,l=R_c$, i.e., at the location of the classical cyclotron orbit. The characteristic width of the maximum in the radial direction is l. Thus, the picture of the electron localized within a narrow ring naturally appears (see Sec. I).

Second, using Eq. (56), the order parameter [Eq. (28)] of a single coherent state can be calculated easily. It is equal to

$$\Delta(q)=\Delta_c(q)\equiv\frac{1}{L_xL_y}\exp\left(-\frac{1}{4}q^2l^2\right). \tag{57}$$

Third, two coherent states centered at points $\boldsymbol{R}_1$ and $\boldsymbol{R}_1$ separated by a distance $r=|\boldsymbol{R_2}-\boldsymbol{R_1}|$, have a very high degree of orthogonality if $r\gg l$. [This is owing to oscillating phase factors not shown in Eq. (56)]. The overlap $A(r)$ between two such states is given by

$$A(r)\equiv|\langle c_{\boldsymbol{R}_1}c^{\dagger}_{\boldsymbol{R}_2}\rangle|^2=\exp\left(-\frac{r^2}{2l^2}\right). \tag{58}$$

As a result, with high accuracy, the order parameter of the HF state (3) of two electrons is simply additive: $\Delta(\boldsymbol{r})\simeq\Delta_c(\boldsymbol{r}-\boldsymbol{R}_1)+\Delta_c(\boldsymbol{r}-\boldsymbol{R}_2)$. This holds for a many-electron state as well, provided that the guiding center separation in each pair of electrons exceeds l. Using Eqs. (34) and (57), we arrive at

$$E_{\rm coh}\simeq\frac{1}{2N_e}\sum_{i\neq j}[(n_i-\overline{\nu_N})g_{\rm HF}(\boldsymbol{R}_i-\boldsymbol{R}_j)(n_j-\overline{\nu_N})]-\frac{\overline{\nu_N}}{2}E_{\rm ex}, \tag{59}$$

where N_e is the total number of electrons, and the quantity $g_{\rm HF}(r)$, defined through its Fourier transform,

$$\tilde{g}_{\rm HF}(q)=\tilde{u}_{\rm HF}(q)e^{-(1/4)q^2l^2}, \tag{60}$$

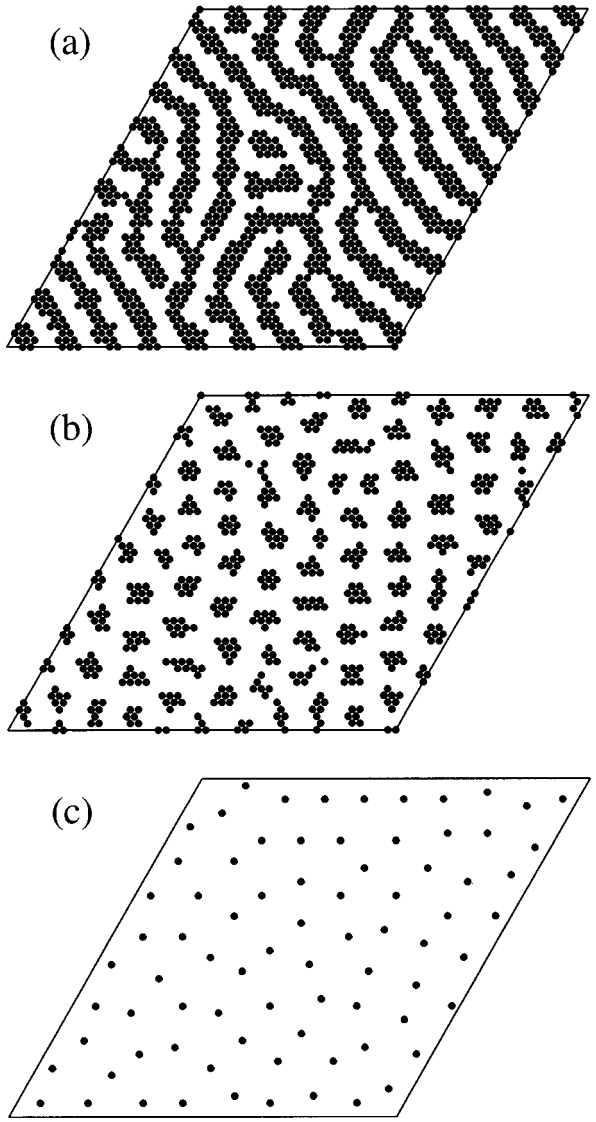

FIG. 9. The CDW patterns produced by our numerical simulations with the parameters $r_s=\sqrt{2}/3$, $N=10$ for three different values of $\overline{\nu_N}$: (a) $\overline{\nu_N}=\frac{1}{2}$, (b) $\overline{\nu_N}=\frac{1}{4}$, (c) $\overline{\nu_N}=\frac{1}{16}$.

has the transparent meaning of the interaction energy of two coherent states whose centers are separated by the distance r. In the actual simulations, we replaced $g_{\rm HF}(r)$ by

$$G_{\rm HF}(r)=\frac{g_{\rm HF}(r)}{1-A(r)} \tag{61}$$

to take into account a nonzero overlap $A(r)$. In fact, the overlap is not too small only for nearest lattice sites, for which $A\approx 0.027$.[30]

In the simulations the lattice had the form of a parallelogram (see Fig. 9) and contained a total of 50×50 sites. In every run, the goal of the simulations was to minimize the energy (59) with respect to different configurations of the given number of the occupied sites, i.e., at given $\overline{\nu_N}$. Since the total number of such configurations is enormous even for a relatively small lattice, the true ground state is extremely hard to find. Fortunately, the Hamiltonian (59) is exactly of the form studied in the context of electrons localized at

charged impurities in doped semiconductors,[31] and we can employ some techniques of finding the approximate solution, developed in that field.

Our computational procedure starts from some initial configuration of the occupied sites (usually a random one). At each step the configuration is changed in favor of a new one with a lower energy. Ideally, the algorithm has to contain many stages with different rules to pick up the new configuration at each stage. At the first stage the new configuration differs from the previous one by the position of only one occupied site; at the second stage, by the positions of the two, and so on. We, however, restricted ourselves to the first stage only. Presumably, it already gives a good approximation to the ground state. The site to move is chosen according to the following procedure. First, we calculate the potentials ϵ_i of all the lattice sites,

$$\epsilon_i = N_e \frac{\partial E_{\rm coh}}{\partial n_i} = \sum_{j \neq i} G_{\rm HF}(\boldsymbol{R}_i - \boldsymbol{R}_j)(n_j - \overline{\nu_N}), \tag{62}$$

and find the occupied site i with the highest potential. Then we scan all the vacant sites j, calculating the quantity

$$\delta E_{i \to j} = \epsilon_j - \epsilon_i - G_{\rm HF}(\boldsymbol{R}_i - \boldsymbol{R}_j), \tag{63}$$

which is the change in the system energy upon the relocation of the occupied site i to the vacant site j.[31] The relocation is performed on the vacant site with the largest positive $\delta E_{i \to j}$. If all $\delta E_{i \to j}$ for the given i are negative, then we try to relocate another occupied site i in the same manner. Eventually, if the pair of an occupied site i and a vacant site j with positive $\delta E_{i \to j}$ cannot be found, the algorithm terminates.

The results of the calculations with the parameters $r_s = \sqrt{2}/3$, $N = 10$, and $\overline{\nu_N} = \frac{1}{2}, \frac{1}{4}, \frac{1}{16}$ are shown in Fig. 9. In Fig. 9(a) one can see that at $\nu_N = \frac{1}{2}$ the stripe pattern forms. The deviations from the ideal picture of identical parallel stripes are mainly due to the incommensurability of the lattice constant with the optimal CDW period. Other factors working in the same direction are the finite size of the lattice and the fact that the algorithm is able to find only an approximation to the ground state. For the same reasons, it is difficult to pinpoint the transition to the ''bubble'' phase. However, we can put some bounds on it. For example, at $N = 10$, the transition occurs within the interval $0.3 < \overline{\nu_N} < 0.4$ (in agreement with our earlier estimate $\nu_N^* = 0.39$). At smaller $\overline{\nu_N}$, the pattern of isolated ''bubbles'' becomes fully developed, see Fig. 9(b).

We found that both the distance between the ''bubbles'' ($\Lambda_b \approx 3.3 R_c$ at $\overline{\nu_N} = \frac{1}{4}$) and the average number of electrons in one ''bubble'' $n_e \approx 3 \overline{\nu_N} N$ are in agreement with the asymptotical laws given by Eq. (55) and the data of Fig. 8. As $\overline{\nu_N}$ goes down, n_e becomes smaller, and, at sufficiently small filling factor ($\overline{\nu_N} \sim 0.1$ for $N = 10$), the ''bubbles'' consist of only single occupied sites. At this moment the distinction between the CDW and the WC disappears. At even smaller $\overline{\nu_N}$, the occupied sites become more distant [Fig. 9(c)].

Summarizing the results discussed in this section, we see that our numerical simulations give an additional piece of evidence in favor of the proposed CDW ground state. In Sec. V we discuss the one-particle DOS of the CDW state and its relation to the recent tunneling experiments.[18]

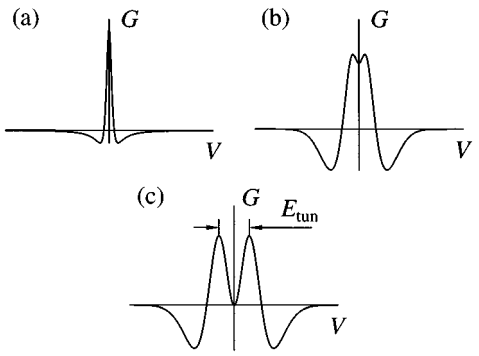

FIG. 10. The evolution of the peak in the differential conductivity $G(V)$ as the magnetic field increases. (a) Shubnikov–de Haas regime. (b) Spin-unresolved QHE regime. (c) Spin-resolved QHE regime.

V. TUNNELING PROPERTIES

In Sec. II we found that the one-particle DOS consists, roughly, of the two Van Hove singularities at the extremes of the spectrum $E = \pm \frac{1}{2} E_g$ with E_g given by Eq. (5). Experimentally, the DOS can be probed by the double-well tunneling experiments.[17,18] We derive the expression for the tunneling conductance as a function of the voltage difference between the two wells and then compare this expression with the experimental results of Ref. 18.

In the tunneling experiments of Refs. 18 and 17 two $\sim$200-Å-thick high-mobility GaAs quantum wells, each containing the 2DEG, are separated by an $Al_xGa_{1-x}As$ barrier of width about 150 Å. The experiment consists in measuring the low-temperature current-voltage characteristics of the double-well system in the magnetic field applied perpendicular to the 2D planes. The results of the experiments (illustrated by Fig. 10) suggest the following scheme: (A) At sufficiently weak magnetic fields the differential conductivity $G = dI/dV$ exhibits a single peak centered at zero bias voltage [Fig. 10(a)]. The form of the peak is consistent with a Lorentzian-type dependence of I on V:[18]

$$\frac{I}{V} = D \frac{2\Gamma}{(eV)^2 + \Gamma^2}, \tag{64}$$

where Γ is the tunneling peak width and D is some constant. (B) At larger magnetic fields the peak broadens and a small depression in G as a function of V at $V = 0$ develops. Thus, the dependence $G(V)$ has two maxima [Fig. 10(b)]. (C) With further increase in the magnitude of the magnetic field, both the total width of the feature and the distance $E_{\rm tun}$ between the two maxima increases. The latter distance appears to be linear in magnetic field,

$$E_{\rm tun} = 0.45 \hbar \omega_c ; \tag{65}$$

see Fig. 10(c).

We are interested mainly in regime C where the magnetic field is not too weak. Nevertheless, for the sake of completeness, we will discuss the other two regimes [(A) and (B)] as well. We associate the existence of the three different regimes [(A), (B), and (C)] with different relations among three energy scales: $\hbar \omega_c$, γ, and $E_{\rm ex} \sim r_s \hbar \omega_c$. They charac-

terize the strength of the magnetic field, the LL broadening due to the disorder, and the strength of the electron-electron interactions, respectively.

(A) *Shubnikov–de Haas regime*. This regime corresponds to the condition $\hbar\omega_c \ll \gamma$, where the dominating energy scale is due to the disorder. In this case the role of the electron-electron interactions reduces mainly to the screening of the impurity potential. Denote the screened potential by $W(\boldsymbol{r})$. The tunneling properties of the system can be adequately analyzed within a simple model of noninteracting electrons in zero magnetic field subjected to the external potential $W(\boldsymbol{r})$. Such a theory leading to formula (64) was developed by Zheng and MacDonald.[32] In the simplest case where the two wells have identical densities, amounts of disorder, and where the disorder in the wells is uncorrelated, the results of Zheng and MacDonald can be understood from a well-known formula (see, e.g., Shrieffer, Scalapino, and Wilson[33]):

$$I = \frac{e}{\hbar^3}\sum_{\boldsymbol{kp}\sigma} |T_{\boldsymbol{kp}}|^2 \int \frac{dE}{2\pi} A^L_{\boldsymbol{k}\sigma}(E) A^R_{\boldsymbol{p}\sigma}(E+eV) \times [f(E)-f(E+eV)]. \tag{66}$$

In this formula $T_{\boldsymbol{kp}}$ is the tunneling matrix element, $A_{\boldsymbol{k}\sigma}(E)$ is the spectral density for energy E, momentum $\hbar\boldsymbol{k}$, and spin σ. The superscripts L and R stand for the left and right wells. Finally, $f(E)$ is the Fermi-Dirac distribution function. Equation (66) shows that the tunneling experiments measure the convolution of the wells' spectral functions.

The most important assumption for the derivation of Eq. (64) (and for the resonant character of zero-bias tunneling in general) is that the momentum is conserved during tunneling, e.g., that $|T_{\boldsymbol{kp}}|^2 \propto \delta_{\boldsymbol{k},\boldsymbol{p}}$. If, following Ref. 32, one now takes advantage of the Born approximation expression

$$A_{\boldsymbol{k}\sigma}(E) = \frac{\hbar^2/\tau}{(E-E_k)^2 + (\hbar/2\tau)^2} \tag{67}$$

for the spectral function, one then recovers Eq. (64) with $\Gamma = \hbar/\tau$. Here, τ is the quantum lifetime and $E_k = \hbar^2 k^2/2m$. As noted above, Eq. (64) describes the experimental results rather well.[18,32,34] However, before we proceed to the case of stronger magnetic fields [regime (B)], we note that in dirtier samples one should observe a different $I(V)$ dependence, owing to the fact that the Born approximation breaks down. We will show that the disorder broadening γ of the LL's, and, consequently, the tunneling peak width, can be much larger than $\hbar/\tau$. To do so, we will need to make several definitions first. In the studied samples the disorder is presumably due to randomly positioned ionized donors. In this case the correlation length of the disorder potential is of the order of spacer width d, which can easily be of the order of 1000 Å. Let n be the 2D electron gas (2DEG) density, and n_i be the density of randomly positioned donors. It is easy to calculate then that the root-mean-square (rms) value of the screened disorder potential in the plane of the 2DEG is equal to[21]

$$U \equiv \sqrt{\langle W^2 \rangle} = \left(\frac{\pi}{8}\right)^{1/2} \frac{e^2 a_B \sqrt{n_i}}{d}. \tag{68}$$

The Born approximation and, consequently, Eq. (64) are valid if $U \ll \hbar v_F/d$, which is the same as $n \gg n_i$. In the opposite case, $n \ll n_i$, one has to use the quasiclassical approximation, which leads to

$$A_{k\sigma}(E) = \frac{\sqrt{2\pi}\hbar}{U} \exp\left[-\frac{(E-E_k)^2}{2U^2}\right] \tag{69}$$

for the spectral function and

$$\frac{I}{V} = \frac{\sqrt{\pi}D}{U} \exp\left[-\frac{(eV)^2}{4U^2}\right] \tag{70}$$

for the tunneling current. Technologically, it is currently possible to change both n and n_i in a given sample. The former may be done by applying a voltage to gates located nearby the quantum wells,[35] and the latter by special techniques of the sample's cooldown.[36] Hence, it is possible to see the crossover from Eq. (64) to Eq. (70) experimentally. In this connection we mention a relation $U = (\hbar/\tau)\sqrt{n}/n_i$, which ensures that the change in the tunneling peak width from $\gamma = \hbar/\tau$ (at $n \gg n_i$) to $\gamma = U$ (at $n \ll n_i$) is continuous.[37] Concluding the consideration of regime A, note that in terms of transport measurements, it corresponds to the Shubnikov–de Haas effect, which is reflected in the name of this regime.[38]

Since the data of Ref. 18 appear to agree with Eq. (64), corresponding to $n \gg n_i$, we will assume this inequality to hold in the following. In this case, regime A can be (somewhat arbitrarily) defined as $\omega_c\tau < \pi$.

(B) *Spin-unresolved quantum Hall effect regime*. When the magnetic field is increased, we switch from regime (A) to regime (B), where $\gamma \ll \hbar\omega_c$ yet $\gamma \gg E_{\rm ex}$. It corresponds to the spin-unresolved quantum Hall effect (QHE) in transport measurements. The LL's with different N are now well defined; however, the disorder is still strong enough to cause the collapse of the spin splitting of the LL spin subbands.[40] Hence, the ground state is not spin polarized, and the CDW at the upper LL does not appear yet.

As in regime (A), the interaction among electrons can be treated on the mean-field level, and the main interaction effect is the screening of the impurity potential. It can be shown that the screening is performed largely by the electrons occupying the lower completely filled LL's and the screened potential $W(\boldsymbol{r})$ is changed little from itself in zero field.[40]

In regime (B), the shape of the tunneling peak is determined by the convolution of the upper LL DOS of the two wells. To show this, in Eq. (66) we switch from (k_x, k_y) to (X, n) (the guiding center coordinate and the LL index) representation. The basis states in this representation are given by Eq. (14). At zero temperature the expression for the tunneling current becomes

$$I = \frac{e}{\hbar^3} T^2 \sum_{Xn\sigma} \int_0^{eV} \frac{dE}{2\pi} A^L_{Xn\sigma}(E-eV) A^R_{Xn\sigma}(E). \tag{71}$$

This equation allows two simplifications. First, at bias voltages $|eV| < \hbar\omega_c$ we have to retain only the terms with $n = N$ in the sum. Second, it is easy to understand that $A_{XN\sigma}(E)$ does not depend on either σ or X. Instead of $A_{XN\sigma}(E)$, it is more convenient to use another quantity, $g(E)$, which depends only on E:

$$g(E)=\frac{1}{2\pi\hbar}A_{XN\sigma}(E). \tag{72}$$

Clearly, $g(E)$ is the DOS at the upper LL. In agreement with our statement above we find that

$$I=2\frac{\pi D\hbar\omega_c}{e}\int_0^{eV}dEg(E-eV)g(E), \tag{73}$$

i.e., that the tunneling current is determined by the convolution of the DOS in the two wells. The factor of two in Eq. (73) accounts for the spin degeneracy. The constant D is the same as in Eq. (64).

The characteristic width γ of LL's has a square-root dependence on the magnetic field,[41]

$$\gamma=\sqrt{\hbar\omega_c\frac{\hbar}{2\pi\tau}}. \tag{74}$$

Owing to the convolution, the width of the tunneling peak is a factor of 2 larger than γ. As for the shape of the tunneling peak, it depends on the relation between the magnetic length l and the correlation length d of the disorder potential.[42]

There is still one more issue to address when considering regime (B). In the experiment, one can see a small depression in $G(V)$ in the vicinity of zero bias [Fig. 10(b)]. Such a depression cannot be explained within the model where the electron-electron interactions are treated on the mean-field level. We think that the observed depression is a manifestation of a correlation effect, namely, the Coulomb gap.[31] At present, the theory of the Coulomb gap is developed only for strongly localized, i.e., almost classical particles. The quantum-mechanical effects have been studied numerically within the Hartree-Fock approximation.[43] It is not clear whether or not the ideas of the classical Coulomb gap are at all applicable to the system we are studying now. If they do, a naive estimate for the characteristic width of the depression will be the energy of the Hartree interaction at the distance of the order of the magnetic length l. This energy is larger than E_h but smaller than $E_{\rm ex}$. For a better estimate, a deeper understanding of the Coulomb gap in the QHE regime is required.

(C) *Spin-resolved QHE regime*. This regime is realized at even stronger magnetic fields where $E_{\rm ex}$ becomes larger than γ.[40] The electron-electron interactions are now the most important, while the disorder can be treated as a weak perturbation.

Depending on how large the ratio n/n_i is, the evolution of the thermodynamical and transport properties of the system undergoes one or multiple stages as the magnetic field increases. To avoid complexity, let us consider only the case $n_i\ll n\ll n_i/\alpha^3$, where $\alpha=E_{\rm ex}/\hbar\omega_c$.

The transition from regime (B) to regime (C) is associated with several dramatic changes.[40] First, the LL's become spin split and in transport measurements one should see spin-resolved conductivity peaks. Second, the nature of screening changes. Now it is performed mainly by the upper LL and it is stronger than in zero magnetic field. As a result, the amplitude of the random potential drops by a factor of the order of α, and $\gamma\to\alpha\gamma$. Thus, in this regime the disorder is additionally suppressed. Third, at the upper spin subband the CDW appears. As a result, the DOS acquires Van Hove singularities separated by a pseudogap of the order of E_g. As for the tunneling current, it is related to the DOS by

$$I=\frac{\pi D\hbar\omega_c}{e}\int_0^{eV}dEg(E-eV)g(E), \tag{75}$$

which differs from Eq. (73) by a factor of 2 due to the fact that the spin degeneracy is lifted. We show below that at moderate N, the differential conductance $G(V)$ exhibits two sharp maxima separated by a pseudogap whose width we denote by $E_{\rm tun}$ [Fig. 10(c)].

Equation (75) shows that the tunneling current is determined by the DOS. In a disorder-free system the DOS is given by

$$g(E)=\frac{2\pi l^2}{L_xL_y}\sum\ \delta(\epsilon_i-E), \tag{76}$$

ϵ_i being the energy levels in the self-consistent HF potential $\epsilon(x,y)$. We will consider the stripe and ''bubble'' phases separately.

A. Stripe phase

In this case the energy levels are given by $\epsilon_i=\epsilon(ia)$, a defined by Eq. (16), which in the limit $L_y\to\infty$ leads to

$$g(E)=\frac{2}{\Lambda}\begin{cases}\left|\dfrac{d\epsilon}{dx}\right|^{-1}, & |E|<\frac{1}{2}E_g\\ 0, & |E|>\frac{1}{2}E_g.\end{cases} \tag{77}$$

We will start with the case of a theoretical interest, $N\gg 1$, where the DOS is schematically shown in Fig. 2. In the first approximation, $g(E)$ vanishes at $|E|<\frac{1}{2}E_h$ and $|E|>\frac{1}{2}E_g$, and so does the tunneling current at bias voltages $|eV|<E_h$ and $|eV|>E_g$. More precisely, at $|eV|<E_h$, the current first precipitously drops towards $V=0$ by a factor of the order of N^2 and then decreases more slowly until at $V=0$ it vanishes entirely. Clearly, at large N the differential conductivity $G(V)$ at $|eV|<E_h$ and $|eV|>E_g$ is very small. Now examine the intermediate range of eV.

At $eV=\pm\frac{1}{2}(E_h+E_g)$ and $eV=\pm E_g$, G exhibits sharp maxima associated with the presence of the delta functions in $g(E)$. Thus, G has four maxima as a function of V, and the distance between the furthermost ones is $2E_g$.

Now let us see how these results are modified by a weak disorder. Recall that the impurity potential $W(\mathbf{r})$ is strongly screened by the electron gas. In general, it is necessary to know how such a screening is achieved. For simplicity, we will discuss only the case of high magnetic fields where $R_c\ll d$. In this case the screening is performed by long-range fluctuations of the electron density at the upper LL. We can say that there is a random distribution of the local filling factor ν_N, described by the probability density $P(\nu_N)$. Clearly, in our model $P(\nu_N)$ is close to the normal distribution

$$P(\nu_N)=\frac{1}{\sqrt{2\pi\delta\nu}}\exp\left[-\frac{(\nu_N-\overline{\nu_N})^2}{2(\delta\nu)^2}\right]. \tag{78}$$

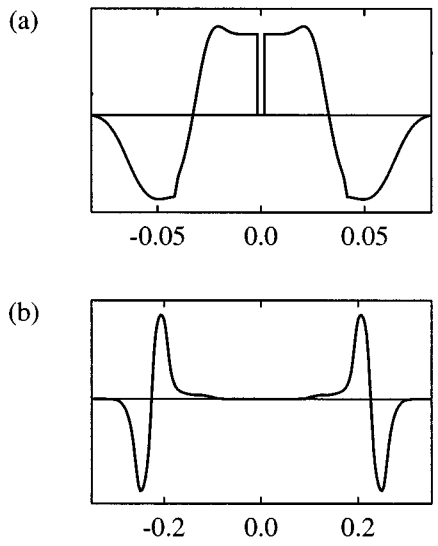

FIG. 11. The differential conductivity G as a function of the bias voltage V. eV (horizontal axes) is in units of $\hbar\omega_c$. (a) $N\gg 1$, (b) $N=3$. The other parameters used in generating these graphs are $r_s=1$, $\overline{\nu_N}=\frac{1}{2}$, and $\delta\nu=0.05$. The calculations are made for the stripe phase.

The characteristic spread $\delta\nu$ of such a distribution can be related to n_i, in its turn related to the width of the tunneling peak $\Gamma=\hbar/\tau$ in zero magnetic field:

$$(\delta\nu)^2=\frac{n_i}{\sqrt{8\pi}(n_L d)^2}=\frac{\sqrt{2}}{r_s}\frac{(e^2/\kappa d)(\hbar/\tau)}{(\hbar\omega_c)^2}. \tag{79}$$

The DOS is given by

$$g(E)=\int_0^1 d\nu_N P(\nu_N) g_0(\nu_N,E), \tag{80}$$

where $g_0(\nu_N,E)$ is the DOS in a disorder-free system for the filling factor ν_N. The energy E is referenced with respect to the Fermi level.

It is clear that the disorder causes smearing of all sharp features in the DOS. Consequently, the main effect of the disorder is the removal of the singularities in $g(E)$ at the extremes of the spectrum. In fact, these singularities have a very small weight [equal to the fraction of the CDW period where $\epsilon(x)=$const, see Fig. 4]. As a result of such a smearing, the sharp maxima in $G(V)$ disappear. The remaining feature has the total spread of $2E_g$ and it is as follows [Fig. 11(a)]. At $|eV|<E_h$, $G(V)\approx 0$; at $E_h<|eV|<\frac{1}{2}(E_h+E_g)$, the differential conductivity is positive and approximately constant. At $|eV|\approx\frac{1}{2}(E_h+E_g)$, $G(V)$ drops sharply, crosses zero, and becomes equal to a negative constant with about the same absolute value. Finally, at $|eV|=E_g$, $G(V)$ rises rapidly to reach zero. In the limit of large N, $E_g\gg E_h$, and so $G(V)$ does not exhibit any sharp maxima. The small ''bumps'' visible in Fig. 11(a) are the only reminders of the distinct Van Hove singularities of the clean case. Clearly, in the dirty case our definition of the tunneling pseudogap becomes very unnatural. It is more logical to associate the pseudogap with the range $-E_h<eV<E_h$ where $G(V)$ is small. As for the larger energy scale E_g, it describes the total width of the tunneling peak.

The described picture applies to the case of large N. However, experimentally accessible N ($1\leqslant N\leqslant 4$) are not large. For such N we calculated $G(V)$ numerically. As an example, the results for $N=3$ are shown in Fig. 11(b) where one can see two sharp maxima in $G(V)$. We found that $E_{\rm tun}$ can be satisfactorily fitted to a linear law $E_{\rm tun}\approx 0.4\hbar\omega_c$. We recall that this expression is obtained for $\overline{\nu_N}=\frac{1}{2}$. In general, $E_{\rm tun}$ decreases more or less linearly as $\overline{\nu_N}$ becomes smaller. At $\overline{\nu_N}\lesssim 1/N$ this dependence becomes sublinear. Eventually, $E_{\rm tun}$ vanishes altogether at $\overline{\nu_N}=0$.

B. ''Bubble'' phase

In this case to obtain the DOS [Eq. (76)] one has to find the self-consistent HF potential $\epsilon(x,y)$ and then solve the Schrödinger equation with this potential to find the energy levels ϵ_i. As in any periodic system, they will form energy bands. Certainly, the stripe phase we studied above is also periodic, and, therefore, its DOS also has a band structure. However, in the case of the stripe pattern there is only one (partially occupied) band, so mentioning the band structure would have been superfluous. On the contrary, for the ''bubble'' phase there are several bands, and their total number depends on the number of flux quanta penetrating a unit cell of the lattice formed by the ''bubbles.'' When this number is not a rational fraction, the band structure becomes a fractal set akin to the celebrated Hofstadter ''butterfly.''[1] However, a small amount of disorder will smear such subtle details in the DOS, leaving only some robust features. The latter can be easily analyzed when N is large and the quasiclassical approximation is adequate.

Recall that every ''bubble'' resides in a potential well created by the HF interaction. Neglect at first the possibility of tunneling into the neighboring wells, then the spectrum is discreet and the quantized energies ϵ_i are simply the energies of the constant energy contours in the self-consistent potential $\epsilon(x,y)$, enclosing an integer number of flux quanta. The difference between the largest and the smallest ϵ_i is of the order of the potential well depth. The tunneling causes the spreading of such discreet levels into the energy bands. However, at large N their widths are exponentially small. Indeed, these widths have the same order of magnitude as the overlap of two coherent states separated by the period of the ''bubble'' lattice, i.e., by the distance of the order $3R_c\gg l$. Hence, at large N the DOS can be approximated by a set of narrow peaks and our predictions for the tunneling experiments are as follows. In a sufficiently clean sample, the differential conductivity exhibits many peaks. The distance in energy between the furthermost peaks is of the order of E_g (as in the case of the stripe pattern). Also, similar to the case of stripes, there exists a gap of width $2E_h$ centered at zero bias. However, unlike in the case of stripes, the current is not just strongly suppressed at $|eV|<E_h$, but vanishes exactly because in this case this is a true gap, not a pseudogap. This concludes our analysis of regime (C).

Previously, the conclusion about the existence of the tunneling gap with the width $2E_h$ was reached in Refs. 9 and 19. However, their predictions for the overall shape of the

DOS are different from ours. Unlike the broad feature with the overall width $E_g \gg E_h$ we derive, their results are that the DOS consists of just two narrow peaks. Thus, the energy scale E_g does not appear in their DOS.

Recently, Levitov and Shytov[20] also argued that the tunneling conductance is represented by two narrow peaks. Let us again use $E_{\rm tun}$ to denote the distance between the peaks in $G(V)$. In our notations, the result of Levitov and Shytov is

$$E_{\rm tun}=2E_{\rm ex}. \tag{81}$$

By $E_{\rm ex}$ in this formula, we mean the exchange gap for the spin excitations in one well for the double-well system. It differs from the one given by Eq. (1), derived for an isolated well, by arguments of the logarithms. [This originates from the difference in the screening properties of a single-well and of the double-well system (see below).] As for a single-well system, $E_{\rm ex}$ is linear in field at large N. Formula (81) was derived in Ref. 20 under an assumption that the dynamics of the system can be described by fluctuations of the Fermi surface. Apparently, in this approach the discreteness of the LL's is lost. It is not accidental then that $E_{\rm tun}$, as given by Eq. (81), does not depend on the filling $\overline{\nu_N}$ of the upper LL. At the same time, it is clear that such dependence does exist. Indeed, consider the $\overline{\nu_N} \ll 1/N$ case where the ground state is a dilute WC. This system can be treated semiclassically with the result that the tunneling gap is equal to twice the energy difference of a vacancy and an interstitial, which is of the order of the Hartree interaction on the distance between nearest neighbors. This energy is much smaller than $E_{\rm ex}$, and, moreover, vanishes altogether in the limit $\overline{\nu_N} \to 0$. More generally, it can be shown that $E_{\rm tun}$ never exceeds $2E_{\rm ex}$, and Eq. (81) holds only in the limit $\overline{\nu_N} \to +0$ in one well, while $\overline{\nu_N} \to 1-0$ in the other. It does not hold in the case of equal densities it was proposed for.

Concluding this section, we discuss briefly the proximity effects, important if the separation b between the two wells is comparable with $a_B \sim 100$ Å. If we go again through the derivation of Eq. (75), keeping in mind that we are examining regime (C) now, it is easy to realize that we, in fact, assumed that any reasonable amount of the disorder would be sufficient for the self-averaging of A_{NX} in the sample and that the phases of the CDW in the two wells are uncorrelated. We also ignored the interaction between the tunneling electron and the hole it leaves behind.[44] Let us examine how such effects can modify our results.

Ideally, when the two wells are brought close together, the CDW patterns existing in each well should lock in the antiphase to reduce the Hartree energy of the system. This can be understood with the example of the limiting case of the two wells located next to each other. In this case the Hartree energy is reduced to zero because the charge oscillations in one well are compensated by the charge oscillations in the other, and the total charge no longer oscillates. This effective suppression of the Hartree potential would lead to an increase in the optimal CDW period. Correspondingly, in the expression (46) for E_g one has to use larger Λ; i.e., E_g tends to increase. However, the phase locking energy, or the difference in energy for the antiphase and in-phase arrangements turns out to be small for the parameters of Ref. 18. We expect that this phase locking effect is totally washed out at experimentally accessible temperatures and amounts of disorder. Therefore, it is more reasonable to assume that the CDW in the two wells are uncorrelated as we did above.

A more important effect is the enhancement of the dielectric constant. It can be shown that for the double-well system the single-well dielectric constant $\varepsilon(q)$ [Eq. (22)] gets replaced by a larger value of

$$\varepsilon(q) \to \varepsilon(q)\frac{e^{2qb}-[1-\varepsilon(q)^{-1}]^2}{e^{2qb}-[1-\varepsilon(q)^{-1}]}. \tag{82}$$

For example, at $b=0$ the dielectric constant roughly doubles. The stronger screening leads to decrease in $E_{\rm tun}$.

Finally, there is also a so-called excitonic shift, which accounts for the interaction between the negatively charged tunneling electron and the positively charged hole it leaves behind. The excitonic shift reduces $E_{\rm tun}$ as well. For example, in the limiting case $b=0$, $E_{\rm tun}$ vanishes altogether. In practice, however, one has the inequality $a_B \ll b \ll R_c$, and the aforementioned effects cause a small correction to $E_{\rm tun}$. Our estimate of such a correction is as follows:

$$E_{\rm tun}(b)=E_{\rm tun}(\infty)-\hbar\omega_c\left[\frac{\ln(2Nr_s\sqrt{a_B/b})}{N}+\frac{\pi r_s}{12\sqrt{2}}\frac{a_B^2}{b^2}\right]. \tag{83}$$

VI. CONCLUSION

In this paper we showed that, in the framework of the Hartree-Fock approximation, the ground state of the 2D electron gas in a weak magnetic field is a CDW at the upper partially filled LL. Both the cohesive energy per electron at the upper LL and the characteristic width of the LL's have the scale of the exchange-enhanced spin splitting of the upper LL. This energy is smaller than $\hbar\omega_c$ for $r_s \lesssim 1$, and thus, the LLs are not destroyed by the electron-electron interaction.

As the magnetic field decreases, the fraction of electrons, participating in the CDW, goes to zero, so that at zero magnetic field the density is uniform.

The existence of the CDW leads to the pseudogap in the one-particle DOS centered at the Fermi energy. The calculated width of the pseudogap seems to be in a good agreement with the width of the pseudogap observed in the tunneling conductance of the double-well system.[18]

The CDW at the upper LL strongly affects the low-temperature transport properties of the 2D gas. Due to the pinning of the CDW by disorder, the dissipative conductivity σ_{xx} has narrow peaks at half-integer fillings even in high-mobility heterostructures. At higher temperatures the depinning of the CDW becomes possible. The effect of this phenomenon on the transport properties remains to be studied. At the moment, we can only estimate the temperature T_c at which the CDW melts into a perfectly uniform electron liquid. In the spirit of Ref. 2, this estimate is

$$k_B T_c=\overline{\nu_N}(1-\overline{\nu_N})\tilde{u}_{\rm ex}(q_0). \tag{84}$$

At $r_s \sim 1$, we can use the asymptotical formula (33) to get

$$k_B T_c\left(\overline{\nu_N}=\frac{1}{2}\right)\approx 0.02\hbar\omega_c+0.06E_h. \tag{85}$$

Above T_c, the pinning effects disappear completely; the peaks in σ_{xx} become wide; the plateaus in σ_{xy} become narrow. At $N=5$, Eq. (85) gives $T_c\approx 0.03\hbar\omega_c$ in reasonable agreement with experimental data.[22,45]

ACKNOWLEDGMENTS

Useful discussions with I. L. Aleiner, L. I. Glazman, D. R. Nelson, and I. M. Ruzin are greatly appreciated. We are grateful to V. J. Goldman and L. P. Rokhinson for communicating to us their unpublished results. This work was supported by NSF under Grant No. DMR-9321417.

APPENDIX A: DERIVATION OF EQ. (43)

Using Eqs. (22), (29), (30), and (40), we find

$$u_{\rm ex}(x)=\frac{\hbar\omega_c}{L_y}\int_0^\infty \frac{dyF^2(r/l^2)}{1+r/\xi-J_0^2(rk_F)}, \tag{A1}$$

$$r\equiv\sqrt{x^2+y^2}. \tag{A2}$$

We will use the following asymptotic formula for $F(q)$, which can be derived by the saddle-point integration in Eq. (25), using the WKB approximation for the wave functions (14) in the integrand:

$$F(q)\simeq\sqrt{\frac{2}{\pi qsR_c}}\cos\left[\frac{qsR_c}{2}+k_FR_c\arcsin\left(\frac{q}{2k_F}\right)-\frac{\pi}{4}\right], \tag{A3}$$

where

$$s\equiv\sqrt{1-(q/2k_F)^2}. \tag{A4}$$

This formula is valid for $qR_c,(2k_F-q)R_c\gg N^{2/3}$. Note that it agrees with Eq. (31) but has a broader region of validity towards large q.

By means of this formula, Eq. (86) can be transformed into

$$u_{\rm ex}(x)\simeq\frac{a\hbar\omega_c}{\pi^2R_c}\int_0^{\sqrt{4R_c^2-x^2}}\frac{{\rm d}y}{r\sqrt{4R_c^2-r^2}(1+r/\xi)}+a\,\delta(x)E_h, \tag{A5}$$

which can be rewritten as

$$u_{\rm ex}^{\rm eff}(x)\simeq a\,\delta(x)E_h+\frac{a\hbar\omega_c}{\pi^2}\int_0^{\sqrt{4R_c^2-x^2}}\frac{dy}{\sqrt{4R_c^2-x^2-y^2}}\times\left(\frac{1}{\sqrt{x^2+y^2}}-\frac{1}{\xi+\sqrt{x^2+y^2}}\right). \tag{A6}$$

On the other hand, the Hartree part for $a_B<|x|<cR_c$, c being a number of order unity, can be approximated by

$$u_H^{\rm eff}(x)=\frac{2}{L_y}\int_0^{\sqrt{4R_c^2-x^2}}dy\,\frac{e^2a_B}{\pi r\kappa\sqrt{4R_c^2-x^2-y^2}}+{\rm const}; \tag{A7}$$

see Eq. (B12) below. Combining the last two equations, we obtain Eq. (43).

APPENDIX B: WIGNER CRYSTAL REVISITED

In this appendix we calculate the cohesive energy $E_{\rm coh}^{\rm WC}$ of the HF WC state and then compare it with the cohesive energy $E_{\rm coh}^{\rm CDW}$ of the CDW state. As explained in Sec. III, our CDW state differs from the WC at $1/(Nr_s^2)\lesssim\overline{\nu_N}\lesssim\frac{1}{2}$. We will show that in this entire range $E_{\rm coh}^{\rm CDW}<E_{\rm coh}^{\rm WC}$; i.e., the CDW state is indeed more energetically favorable. The qualitative arguments in favor of this statement were given in Sec. II.

Earlier, the cohesive energy $E_{\rm coh}^{\rm WC}$ of the WC has been calculated in Ref. 9. For $\overline{\nu_N}<1/N$ our results agree with Ref. 9. At larger $\overline{\nu_N}$, they differ.

To calculate $E_{\rm coh}^{\rm WC}$ we have to find the set of $\Delta(\boldsymbol{q})$ corresponding to the WC state, and then substitute them into the general formula (34). Using Eq. (57), the additivity of order parameter (see Sec. IV), and the Poisson summation formula, it is easy to obtain that nonzero $\Delta(\boldsymbol{q})$ correspond to the wavevectors of the reciprocal lattice of the WC

$$\boldsymbol{q}_{i,j}=Q_0\left(i+\frac{1}{2}j,\frac{\sqrt{3}}{2}j\right),\quad Q_0=\sqrt{\frac{4\pi\overline{\nu_N}}{\sqrt{3}}}\frac{1}{l}, \tag{B1}$$

for which q they are given by

$$\Delta(q)=\overline{\nu_N}\exp\left(-\frac{1}{4}q^2l^2\right), \tag{B2}$$

derived earlier in Ref. 3 for the WC at the lowest LL. Hence, for the cohesive energy of the WC we obtain

$$E_{\rm coh}^{\rm WC}=\frac{\overline{\nu_N}n_{\rm L}}{2}\sum_{|i|+|j|>0}\widetilde{u}_{\rm HF}(\boldsymbol{q}_{i,j})\exp\left(-\frac{1}{2}\boldsymbol{q}_{i,j}^2l^2\right). \tag{B3}$$

1. $\overline{\nu_N}=1/2$

At $\overline{\nu_N}=1/2$ the contribution of the six shortest reciprocal lattice vectors $(i,j)\in\{(\pm1,0),(0,\pm1),(1,-1),(-1,1)\}$ constitutes more than 97% of the sum (B3). Therefore, with a good accuracy one can write

$$E_{\rm coh}^{\rm WC}=\frac{3}{2}n_L\widetilde{u}_{\rm HF}(Q_0)e^{-\pi/\sqrt{3}}, \tag{B4}$$

$$Q_0=\sqrt{\frac{2\pi}{\sqrt{3}}}\frac{1}{l}. \tag{B5}$$

Analyzing this expression, we discover a remarkable fact that $E_{\rm coh}^{\rm WC}$ can be positive. In other words, the WC loses competition even to the uniform electron liquid. Indeed, consider the limit $N\gg r_s^{-2}\gg1$. It follows from Eqs. (32) and (33) that at $q\sim Q_0\sim l^{-1}$ the HF potential is dominated by the (nonnegative) Hartree potential $\widetilde{u}_H(q)$ exhibiting oscillations in q. Roughly, the oscillating part of $\widetilde{u}_H(q)$ is proportional to $\sin(2qR_c)$. Since different N correspond to different values of $\sin(2Q_0R_c)$, $E_{\rm coh}^{\rm WC}$ oscillates as well. For example, if $\sin(2Q_0R_c)=-1$, or, more precisely, if Q_0 is one of the zeros of form factor $F(q)$, the Hartree term $\widetilde{u}_H(Q_0)$ is also zero. In this case $E_{\rm coh}^{\rm WC}$ has a minimum and its value is negative. On

the other hand, if Q_0 coincides with a maximum of $F(q)$, then the HF potential and, consequently, $E_{\rm coh}^{\rm WC}$ are both positive.

The quantity $\sin(2Q_0R_c)$ is a pseudorandom function of N. Its average value within an interval $N\in(r_s^{-2},N_{\max})$ tends to zero as $N_{\max}\to\infty$. Hence, roughly at every other N the cohesive energy $E_{\rm coh}^{\rm WC}$ is positive and the WC (at least, with the triangular lattice) at $\overline{\nu_N}=\frac{1}{2}$ is absolutely unstable.

Nevertheless, there exist N at which $E_{\rm coh}^{\rm WC}$ is negative, and the lower bound for $E_{\rm coh}^{\rm WC}$ can be found assuming that Q_0 coincides with a zero of the Hartree potential. In this case $\tilde{u}_{\rm HF}(Q_0)=-\tilde{u}_{\rm ex}(Q_0)$. Using Eqs. (33) and (B4), one obtains

$$\min\{E_{\rm coh}^{\rm WC}\}\approx -0.01\frac{\hbar\omega_c}{\sqrt{N}}-\frac{E_h}{4}. \tag{B6}$$

This result should be compared with the energy of the CDW state given by Eq. (4). The last term in the two formulas are identical. In fact, it is common for any low-energy state at the Nth LL at $\overline{\nu_N}\gtrsim 1/N$ (see Sec. II). Therefore, we have to compare only the remaining terms. These other terms are negative in both $E_{\rm coh}^{\rm WC}$ and $E_{\rm coh}^{\rm CDW}$. In the limit $N\gg r_s^{-2}$ we are considering now, the absolute value of the term for the CDW state is much larger than of that for the WC state. Hence, the CDW state is more energetically favorable. In addition to the analytical arguments, we also compared $E_{\rm coh}^{\rm WC}$ and $E_{\rm coh}^{\rm CDW}$ numerically. We found that $E_{\rm coh}^{\rm CDW}$ is always smaller than $E_{\rm coh}^{\rm WC}$ in the parameter range of interest: $1\leqslant N\leqslant 10$ and $0.14<r_s<1.2$. However, at such rather moderate N, the difference between the two is not too large (of the order of 5%).

2. $\overline{\nu_N}\ll 1/2$

In this subsection we will consider only the limit $N\gg r_s^{-2}\gg 1$. In principle, we can continue using the general formula (95). However, to give our analysis a new angle, we choose to use formula (59), which, in the case of the WC, is nothing more than the standard lattice sum:[9,14]

$$E_{\rm coh}^{\rm WC}=\frac{1}{2}\sum_{\boldsymbol{R}_i\neq 0} g_{\rm HF}(\boldsymbol{R}_i)-\frac{\overline{\nu_N}n_L}{2}\int \mathbf{d}^2\boldsymbol{r}\, g_{\rm HF}(\boldsymbol{r}). \tag{B7}$$

The conventional estimate of such a lattice sum is

$$E_{\rm coh}^{\rm WC}\sim -\frac{\overline{\nu_N}n_L}{2}\int_{\rm WS}\mathbf{d}^2\boldsymbol{r}\, g_{\rm HF}(\boldsymbol{r})\sim -\frac{1}{2}g_{\rm HF}(a_0), \tag{B8}$$

where the integration is performed over the area of the Wigner-Seitz cell. This is how the results of Ref. 9 have been obtained. As long as the interaction potential $g_{\rm HF}(r)$ is sufficiently smooth at $r\gtrsim a_0$, a_0 being the lattice constant, this procedure is correct. It can be shown, however, that at large N the potential $g_{\rm HF}(r)$ is given by [compare with Eq. (53)]

$$g_{\rm HF}(r)\sim\frac{e^2a_B}{\pi\kappa r\sqrt{4R_c^2-r^2}}+E_h,\quad r\gtrsim\xi,\quad 2R_c-r\gtrsim l, \tag{B9}$$

i.e., it has a sharp maximum at $r=2R_c$ corresponding to the separation at which the cyclotron orbits of the two states start intersecting. It is due to this sharp maximum the Fourier transform of the HF potential oscillates with the period $1/(2R_c)$.

Let us derive Eq. (B9). First of all, note that $\tilde{g}_{\rm HF}(q)$ deviates from $\tilde{u}_{\rm HF}(q)$ only at $q\gtrsim l^{-1}$ [Eq. (60)]; hence, in real space these two potentials essentially coincide at $r\gtrsim l$. Secondly, the exchange potential $u_{\rm ex}(r)$ decays rapidly at distances r larger than $\xi=\sqrt{2}r_sR_c$ (see Sec. III) and soon becomes much smaller than the Hartree potential; therefore,

$$g_{\rm HF}(r)\sim u_H(r),\quad r\gtrsim\xi. \tag{B10}$$

According to Eqs. (29),

$$u_H(r)=\int\frac{\mathbf{d}^2\boldsymbol{q}}{(2\pi)^2}e^{i\boldsymbol{q}\cdot\boldsymbol{r}}\tilde{v}(\boldsymbol{q})F^2(\boldsymbol{q}). \tag{B11}$$

At $\boldsymbol{q}$ yielding the dominant contribution to this integral, $\tilde{v}(\boldsymbol{q})$ can be replaced by $\pi e^2a_B+(2\pi)^2E_h\delta(\boldsymbol{q})$ [cf. Eq. (17)]. Using also Eq. (31) for $F(\boldsymbol{q})$, we arrive at

$$\begin{aligned}u_H(r)&\approx\pi e^2a_B\int\frac{\mathbf{d}^2\boldsymbol{q}}{(2\pi)^2}e^{i\boldsymbol{q}\cdot\boldsymbol{r}}J_0^2(qR_c)+E_h\\&=\frac{e^2a_B}{\pi\kappa r\sqrt{4R_c^2-r^2}}+E_h,\end{aligned} \tag{B12}$$

which together with Eq. (B10) leads to Eq. (B9).

Note that $u_H(r)$ satisfies the relation

$$u_H(r)=n_L\tilde{u}_{\rm ex}(r/l^2), \tag{B13}$$

which follows from Eq. (30). One may wonder why $u_{\rm ex}(q)$ as given by Eq. (33) does not show the inverse square-root singularity present in $u_H(r)$ according to Eq. (B12). It is easy to see, though, that the singularity in $u_{\rm ex}(q)$ is located at $q=2k_F$, which is beyond the limited range of q, for which Eq. (33) is written. Using the relation $\hbar\omega_c=e^2a_B/\kappa l^2$, one can verify that Eq. (B12) does agree with Eq. (33) in the indicated range of q.

Let us now return to the calculation of the cohesive energy of the WC. Depending on the lattice constant a_0, one can distinguish two possibilities: $a_0\gg 2R_c$ ($\overline{\nu_N}\ll 1/N$) and $a_0\ll 2R_c$ ($1/N\ll\overline{\nu_N}\ll\frac{1}{2}$). In the former case the singular part of $g_{\rm HF}(r)$ has no effect and $E_{\rm coh}^{\rm WC}$ can be estimated with the help of Eq. (B8). In the latter case this standard procedure fails. This case requires a more accurate treatment of the lattice sites $\boldsymbol{R}_i$ in Eq. (B7) enclosed by the circle of radius $2R_c$. This can be done as follows.

We divide the entire area of the circle into narrow concentric rings of width δr and then sum the contributions to $E_{\rm coh}^{\rm WC}$ from all rings. Denote by $M(r)$ the number of lattice sites in the ring with inner radius r and outer radius $r+\delta r$. Generally, $M(r)$ is a pseudorandom function of r with the average value of $\overline{M(r)}=2\pi r\,\delta r\,\overline{\nu_N}n_{\rm L}$. Clearly, the contribution of the ring under consideration to $E_{\rm coh}^{\rm WC}$ is $\frac{1}{2}g_{\rm HF}(r)[M(r)-\overline{M(r)}]$. The largest contribution comes from rings with $r\sim 2R_c$ where $g_{\rm HF}(r)$ has the maximum. In order for our procedure to make sense the rings must contain at least one lattice site on average. On the other hand, the accuracy of the estimate is higher if the rings are as narrow

as possible. Hence, the width of the rings δr has to be determined from the condition $\overline{M(2R_c)}\sim 1$, which yields

$$\delta r \sim a_0^2/(4\pi R_c). \tag{B14}$$

Since $M(r)$ is pseudorandom, and the total number of rings $\sim R_c/\delta r$ is finite, $E_{\rm coh}^{\rm WC}$ is also a pseudorandom quantity. In other words, for any given $\overline{\nu_N}$, the cohesive energy $E_{\rm coh}^{\rm WC}$ experiences fluctuations as a function of the ratio R_c/a_0, i.e., as a function of N. This is exactly the conclusion we came to in the preceding subsection by using different arguments. In can be verified that the root-mean-square (rms) value of $E_{\rm coh}^{\rm WC}$ fluctuations is much larger than its average value given by Eq. (B8); therefore, $\min E_{\rm coh}^{\rm WC}$ can be estimated as rms value of $E_{\rm coh}^{\rm WC}$ taken with the negative sign. To proceed we need to know the statistical properties of the pseudorandom quantity $\delta M(r)\equiv M(r)-\overline{M(r)}$. This is an interesting mathematical problem in itself. A related problem, namely, the fluctuations in the number of the square lattice sites contained in a circle as a function of its radius, was studied by many mathematicians starting in the last century.[46] The complete solution has not yet been obtained. However, extensive numerical data indicate that, provided $\delta r < a_0$, (i) the rms value of $\delta M(r)$ is of order $\overline{M(r)}$ and (ii) the fluctuations in $\delta M(r)$ and $\delta M(r+\Delta r)$ can be considered to be statistically independent if $\Delta r < a_0$. In other words, the distribution of the lattice sites within any ring of width a_0 resembles the completely random Poisson distribution. However, the fluctuations in any two such rings are correlated. Clearly, the ring $2R_c - a_0 < r < 2R_c$ gives the dominating contribution to the fluctuations in $E_{\rm coh}^{\rm WC}$ because in this ring $g_{\rm HF}(r)$ reaches its maximum. This leads to the estimate

$$(\min E_{\rm coh}^{\rm WC})^2 \sim \sum_{j=0}^{a_0/\delta r} g_{\rm HF}^2(r)\overline{M}(2R_c - j\,\delta r) \sim \frac{\overline{M(2R_c)}}{\delta r}\int_{\delta r}^{a_0} dr\, g_{\rm HF}^2(2R_c - r). \tag{B15}$$

Evaluating this integral with the help of Eq. (B9), we get

$$\min E_{\rm coh}^{\rm WC} \sim -\hbar\omega_c\left(\frac{\overline{\nu_N}}{N}\right)^{1/2}\ln^{1/2}\left[\frac{a_0}{\max(\delta r, l)}\right]. \tag{B16}$$

Recall that we are considering the case $1/N \ll \overline{\nu_N} \ll \frac{1}{2}$. As one can see, at the upper limit it agrees (up to a numerical factor) with the result obtained earlier for $\overline{\nu_N} = \frac{1}{2}$ [Eq. (B6)].

Finally, the results for different $\overline{\nu_N}$ may be summarized in the following way:

$$\frac{|E_{\rm coh}^{\rm WC}|}{\hbar\omega_c} \lesssim \begin{cases} r_s\sqrt{\overline{\nu_N}N}, & \overline{\nu_N} \ll \dfrac{1}{N^3 r_s^2} \\ \dfrac{\ln(\overline{\nu_N}N^3 r_s^2)}{N}, & \dfrac{1}{N^3 r_s^2} \ll \overline{\nu_N} \ll \dfrac{1}{N} \\ \left(\dfrac{\overline{\nu_N}}{N}\right)^{1/2}\ln^{1/2}(\overline{\nu_N}N), & \dfrac{1}{N} \ll \overline{\nu_N} \ll \dfrac{1}{\sqrt{N}} \\ \left(\dfrac{\overline{\nu_N}}{N}\right)^{1/2}\ln^{1/2}\left(\dfrac{1}{\overline{\nu_N}}\right), & \dfrac{1}{\sqrt{N}} \ll \overline{\nu_N} \ll \dfrac{1}{2}. \end{cases} \tag{B17}$$

At this point we can compare the energies of the WC and the CDW [Eqs. (50) and (B17), respectively] at $1/(Nr_s^2) \ll \overline{\nu_N} \ll \frac{1}{2}$ where Eq. (50) holds. We see that the CDW state wins over the WC in this entire interval.

[1] *The Quantum Hall Effect*, edited by R. E. Prange and S. M. Girvin (Springer-Verlag, New York, 1990).

[2] H. Fukuyama, P. M. Platzman, P. W. Anderson, Phys. Rev. B **19**, 5211 (1979).

[3] D. Yoshioka and H. Fukuyama, J. Phys. Soc. Jpn. **47**, 394 (1979); D. Yoshioka and P. A. Lee, Phys. Rev. B **27**, 4986 (1983).

[4] R. B. Laughlin, Phys. Rev. Lett. **50**, 1395 (1983).

[5] S. L. Sondhi, A. Karlhede, S. A. Kivelson, and E. H. Rezayi, Phys. Rev. B **47**, 16 419 (1993).

[6] A. A. Koulakov, M. M. Fogler, and B. I. Shklovskii, Phys. Rev. Lett. **76**, 499 (1996).

[7] L. Belkhir and J. K. Jain, Solid State Commun. **94**, 107 (1995); R. Morf and N. d'Ambrumenil, Phys. Rev. Lett. **74**, 5116 (1995).

[8] X.-G. Wu and S. L. Sondhi, Phys. Rev. B **51**, 14 725 (1995).

[9] I. L. Aleiner and L. I. Glazman, Phys. Rev. B **52**, 11 296 (1995).

[10] J. F. Janak, Phys. Rev. **174**, 1416 (1969); T. Ando and Y. Uemura, J. Phys. Soc. Jpn. **35**, 1456 (1973).

[11] In Ref. 9 this term in $E_{\rm ex}$ is neglected. It gives only a small correction in the limit $N \gg r_s^{-2} \gg 1$ they considered.

[12] R. J. Nicholas, R. J. Haug, K. v. Klitzing, and G. Weimann, Phys. Rev. B **37**, 1294 (1988); A. Usher, R. J. Nicholas, J. J. Harris, and C. T. Foxton, *ibid.* **41**, 1129 (1990).

[13] S. Kivelson, C. Kallin, D. P. Arovas, and J. R. Schrieffer, Phys. Rev. B **36**, 1620 (1987).

[14] K. Maki and X. Zotos, Phys. Rev. B **28**, 4349 (1983).

[15] For review, see M. Seul and D. Andelman, Science **267**, 476 (1995).

[16] R. C. Ashoori, J. A. Lebens, N. P. Bigelow, and R. H. Silsbee, Phys. Rev. Lett. **64**, 681 (1990).

[17] J. P. Eisenstein, L. N. Pfeiffer, and K. W. West, Phys. Rev. Lett. **69**, 3804 (1992); Surf. Sci. **305**, 393 (1994).

[18] N. Turner, J. T. Nicholls, K. M. Brown, E. H. Linfield, M. Pepper, D. A. Ritchie, and G. A. C. Jones (unpublished); K. M. Brown, N. Turner, J. T. Nicholls, E. H. Linfield, M. Pepper, D. A. Ritchie, and G. A. C. Jones, Phys. Rev. B **50**, 15 456 (1995).

[19] I. L. Aleiner, H. U. Baranger, and L. I. Glazman, Phys. Rev. Lett. **74**, 3435 (1995).

[20] L. S. Levitov and A. V. Shytov (unpublished).

[21] A. L. Efros, Solid State Commun. **65**, 1281 (1988); **67**, 1019 (1989); **70**, 253 (1989).

[22] H. L. Stormer, K. W. Baldwin, L. N. Pfeiffer, and K. W. West, Solid State Commun. **84**, 95 (1992).

[23] D. B. Chklovskii, B. I. Shklovskii, and L. I. Glazman, Phys. Rev. B **46**, 4026 (1992); **46**, 15 606(E) (1992); D. B. Chklovskii, K. A. Matveev, and B. I. Shklovskii, *ibid.* **47**, 12 605 (1993).

[24] D.-H. Lee, Z. Wang, and S. Kivelson, Phys. Rev. Lett. **70**, 4130 (1993); D. B. Chklovskii and P. A. Lee, Phys. Rev. B **48**, 18 060 (1993).

[25] I. S. Gradshtein and I. M. Ryzhik, *Tables of Integrals, Series, and Products* (Academic, Boston, 1994).

[26] A. H. MacDonald and G. C. Aers, Phys. Rev. B **34**, 2906 (1986).

[27] I. V. Kukushkin, S. V. Meshkov, and V. B. Timofeev, Usp. Fiz. Nauk **155**, 219 (1988) [Sov. Phys. Usp. **31**, 511 (1988)].

[28] C. de C. Chamon and X. G. Wen, Phys. Rev. B **49**, 8227 (1994).

[29] To determine the order of the transition, we have considered an alternative (second-order transition) scenario, which is as follows. First, at certain $\overline{\nu_N} > \nu_N^*$, the width of the stripes acquires a periodic modulation in y. As $\overline{\nu_N}$ decreases, the amplitude of the modulation increases. Eventually, at $\overline{\nu_N} = \nu_N^*$, the stripes break into isolated ''bubbles.'' We have found, however, that the modulation decribed above first arises at $\overline{\nu_N} = 0.375$, which is smaller than $\overline{\nu_N} = 0.39$ where the first-order transition occurs. Thus, the second-order transition scenario is not realized.

[30] Strictly speaking, due to a nonzero overlap the energy of the system is not reduced to the sum of solely two-particle interaction energies. However, this appears to be a small effect (Ref. 14).

[31] B. I. Shklovskii and A. L. Efros, *Electronic Properties of Doped Semiconductors* (Springer, New York, 1984).

[32] L. Zheng and A. H. MacDonald, Phys. Rev. B **47**, 10 619 (1993).

[33] J. R. Shrieffer, D. J. Scalapino, and J. W. Wilkins, Phys. Rev. Lett. **10**, 336 (1963).

[34] S. Q Murphy, J. P. Eisenstein, L. N. Pfeiffer, and K. W. West, Phys. Rev. B **52**, 14 825 (1995).

[35] I. Glozman, C. E. Johnson, and H.-W. Jiang, Phys. Rev. Lett. **74**, 594 (1995).

[36] E. Buks, M. Heiblum, and Hadas Shtrikman, Phys. Rev. B **49**, 14 790 (1994); E. Buks, M. Heiblum, Y. Levinson, and Hadas Shtrikman, Semicond. Sci. Technol. **9**, 2031 (1994).

[37] The tails of the tunneling peak in both cases are neither Lorentzian nor Gaussian but rather very nearly exponential: $\ln[G(V)/G(0)] \sim -eV/\gamma_0$. Here $\gamma_0 \sim U^2\tau/\hbar$. This asymptotical behavior holds at $eV \gg \gamma_0$ in the ''quantum'' case $n \gg n_i$ and at $eV \gg \hbar/\tau$ in the ''quasiclassical'' case $n \ll n_i$. Thus, at the cross-over point $n \sim n_i$, the exponential dependence is to be observed in the entire range of bias voltages.

[38] In the ''quantum'' case, $n \gg n_i$, the Shubnikov–de Haas oscillations are described by the Dingle formula, $\delta\rho_{xx}/\rho_{xx}^0 \propto -e^{-\pi/\omega_c\tau}\cos(\pi\nu)$, which applies when $\omega_c\tau \lesssim \pi$. (The temperature is assumed to be low enough.) In the ''quasiclassical'' case, $n \ll n_i$, the QHE effect gives way to Shubnikov–de Haas oscillations at $\hbar\omega_c \lesssim \pi U$. It is interesting to note that the conventional Dingle law holds only at much weaker magnetic fields, $\hbar\omega_c \ll (\hbar v_F/d)$. In the intermediate range, $(\hbar v_F/d) \ll \hbar\omega_c \ll U$, the Dingle law is replaced by a different formula (Ref. 39): $\delta\rho_{xx}/\rho_{xx} \propto -e^{-2\pi^2 U^2/\hbar^2\omega_c^2}\cos(\pi\nu)$. Recently, this dependence has been indeed found in the experiment [P. T. Coleridge (private communication)].

[39] A. G. Aronov, E. Altshuler, A. D. Mirlin, and P. Wöffle, Phys. Rev. B **52**, 4708 (1995); A. D. Mirlin, E. Altshuler, and P. Wölfle (unpublished).

[40] M. M. Fogler and B. I. Shklovskii, Phys. Rev. B **52**, 17 366 (1995).

[41] M. E. Raikh and T. V. Shahbazyan, Phys. Rev. B **47**, 1522 (1993).

[42] If $l \ll d$, the theory of Raikh and Shahbazyan (Ref. 41) applies. The LL's have a Gaussian form [similar to Eq. (69)]. In the opposite case, $l \gg d$, the SCBA (self-consistent Born approximation) is valid and the LL's have a semielliptic form (see Ref. 41 and references therein).

[43] S.-R. Eric Yang and A. H. MacDonald, Phys. Rev. Lett. **70**, 4110 (1993).

[44] In strong magnetic fields, this effect has been experimentally studied by J. P. Eisenstein, L. N. Pffeifer, and K. W. West, Phys. Rev. Lett. **74**, 1419 (1995).

[45] L. P. Rokhinson, B. Su, and V. J. Goldman, Solid State Commun. **96**, 309 (1995); L. P. Rokhinson and V. J. Goldman (unpublished).

[46] See P. M. Bleher, Z. Cheng, F. J. Dyson, and J. L. Lebowitz, Commun. Math. Phys. **154**, 433 (1993).